Contents

1

Sampling Theory and Parallel-Beam Tomography

Adel Faridani

ABSTRACT This article contains a tutorial on the interaction between sampling theory and tomography as well as some new results. We explore how sampling theorems are used in tomography to identify efficient data acquisition schemes; facilitate an error analysis for reconstruction algorithms; and provide a qualitative understanding of some image artifacts. On the other hand, applications in tomography have stimulated research on new estimates for the aliasing error and in non-equidistant sampling theory. New results are included in an analysis of artifacts caused by undersampling.

1 Introduction

Computed tomography (CT) entails the reconstruction of a function f from a finite number of line integrals of f. A natural question to ask is how many and which line integrals should be measured in order to achieve a certain accuracy in the reconstruction. Sampling theory comes naturally into play when trying to answer this question. It turns out that sampling theory is not only useful in identifying efficient sampling schemes for tomographic data, but also provides a qualitative understanding of certain artifacts and facilitates the numerical analysis of reconstruction algorithms. We will explore these themes in the subsequent sections. On the other hand, applications in tomography have stimulated research in sampling theory, for example on estimates for the aliasing error and on non-equidistant sampling.

The article is organized as follows. In the next section we begin by introducing the two-dimensional Radon transform, the mathematical model underlying tomography, and briefly describe how it arises. In § 3 we present the relevant classical sampling theorem and prove the standard estimate for the aliasing error. The section concludes with an improved estimate and an outline of key ideas for its proof. In sections 4 and 5 we describe how to apply the sampling theory of § 3 to tomography in order to identify efficient sampling schemes. A key theme here is that we have a two-dimensional sampling problem and that the particular shape of the support of the Fourier transform of the data must be exploited in order to find efficient sampling schemes.

§ 6 is concerned with reconstruction from efficiently sampled data. This re-

quires some care, and the necessary insights are provided by an error analysis of a reconstruction algorithm. While these first six sections are expository in nature, new results are included in § 7 where we investigate the consequences of undersampling. We first show that elementary sampling theory provides a qualitative understanding why some sampling schemes are more sensitive to undersampling than others. We then present a numerical analysis of the filtered backprojection algorithm which reveals the location and relative strength of some artifacts.

The article concludes with references to further developments.

2 The two-dimensional Radon transform

The two-dimensional Radon transform maps a density function f into its line integrals.

Let $\mathbb{Z}, \mathbb{R}, \mathbb{C}$ denote the integers, real and complex numbers, respectively. Throughout this paper we will assume that $f \in C_0^\infty(\Omega)$, i.e., f is infinitely differentiable and vanishes outside the unit disk Ω of $\mathbb{R}^2$. This assumption simplifies the mathematical proofs, and although the density functions occurring in practice are not necessarily smooth, we will see that our theoretical results describe the phenomena observed in practice well.

Let $\theta = (\cos\varphi, \sin\varphi)$ be the unit vector in $\mathbb{R}^2$ with polar angle φ, and $\theta^\perp = (-\sin\varphi, \cos\varphi)$. For $f \in C_0^\infty(\Omega)$ define its Radon transform Rf by

$$\begin{aligned} Rf(\varphi, s) &= \int_{-\infty}^{\infty} f(s\cos\varphi - t\sin\varphi, s\sin\varphi + t\cos\varphi)dt \\ &= \int_{\mathbb{R}} f(s\theta + t\theta^\perp)dt, \end{aligned} \tag{2.1}$$

i.e., $Rf(\varphi, s)$ is the integral of f over the line in direction $\theta^\perp$ with signed distance s from the origin. Sometimes Rf is considered as a function of s for fixed φ. In this case we write $R_\varphi f(s)$ for $Rf(\varphi, s)$.

In x-ray tomography the Radon transform arises as follows. The function $f(x)$ to be reconstructed is the so-called x-ray absorption coefficient. Since it varies for different materials and tissues, it does provide an image of the interior of an object. We confine ourselves to two dimensions so that the goal is to image a crossection of the object under investigation. Assume a very thin x-ray beam is sent through such a crossection, traveling along a segment of the line $x = s\theta + t\theta^\perp$, $t \in \mathbb{R}$. Then its initial intensity I_0 and its intensity I_1 after passing through the object are related by

$$I_0 = I_1\, e^{-Rf(\theta, s)}.$$

Sending many such rays through the crossection under investigation and measuring each time I_0 and I_1 yields a number of sampled values of Rf. The goal is then to reconstruct an approximation to $f(x)$ from these values. Naturally, one would like to achieve high resolution with a minimal amount of measured data. Thus sampling theory comes into play.

The Fourier transform of a function $g \in C_0^\infty(\mathbb{R}^n)$ is defined by

$$\hat{g}(\xi) = (2\pi)^{-n/2} \int_{\mathbb{R}^n} g(x) e^{-i\langle x,\xi\rangle} dx$$

and is extended to larger classes of functions or distributions by continuity or duality. Here $\langle x, \xi\rangle$ denotes the usual inner product in $\mathbb{R}^n$.

In particular, the Fourier transform of $R_\varphi f$ is given by

$$(R_\varphi f)^\wedge(\sigma) = (2\pi)^{-1/2} \int_{\mathbb{R}} R_\varphi f(s) e^{-is\sigma} ds.$$

The following relation between the Fourier transforms of $R_\varphi f$ and f is easy to verify but very useful:

$$(R_\varphi f)^\wedge(\sigma) = (2\pi)^{1/2} \hat{f}(\sigma\theta). \tag{2.2}$$

Equation (2.2) is called the projection-slice theorem.

For readers inteersted in a more detailed introduction to tomography we recommend the monographs [19, 23] or the introductory surveys [10, 13] and the references given there.

3 Sampling lattices for the Radon Transform

From (2.1) we see that Rf is a function with domain $[0, 2\pi) \times \mathbb{R}$. The subsequent analysis of sampling and resolution will make use of Fourier analysis. This requires both the domain of Rf as well as the sampling sets to have a group structure. Equipped with addition modulo 2π the interval $[0, 2\pi)$ becomes a group, called the circle group, which we denote by $\mathbb{T}$. Then the domain of Rf may be identified with the group $\mathbb{T} \times \mathbb{R}$. The addition on $\mathbb{T} \times \mathbb{R}$ can be viewed as the usual addition in $\mathbb{R}^2$ but modulo 2π in the first component.

The task of tomography is to reconstruct f from finitely many measurements of Rf. In the parallel-beam sampling geometry a set of angles $\{\varphi_j, j = 0, \ldots, P-1\}$ is selected and for each angle φ_j a number of line integrals $Rf(\varphi_j, s_{jl})$ are measured. We require the set $\{\varphi_j, s_{jl}\}$ of all points where Rf is measured to be a subgroup of $\mathbb{T} \times \mathbb{R}$, and for practical reasons there should be more than one measured line for each occurring angle φ_j. A sampling set satisfying these two requirements is called an admissible sampling lattice. The admissible lattices may be parameterized as follows [12]:

Lemma 1. *Let* $\mathbf{L}$ *be an admissible sampling lattice. Then there is* $d > 0$ *and integers* N, P*, such that* $0 \le N < P$ *and*

$$\begin{aligned} \mathbf{L} &= \mathbf{L}(d, N, P) \\ &= \{(\varphi_j, s_{jl}) : \varphi_j = 2\pi j/P,\ s_{jl} = d(l + jN/P), \\ &\qquad j = 0, \ldots, P-1;\ \ l \in \mathbb{Z}\}. \end{aligned} \tag{3.3}$$

From (3.3) we see that there are P directions θ_j corresponding to the equidistant angles $\varphi_j = 2\pi j/P$. For each direction integrals over an equidistant set of lines with spacing d are measured. This collection of equidistant parallel lines is shifted by an amount djN/P which varies with the angle φ_j.

The most important lattices are the standard lattice

$$\mathbf{L}_S = \{(\varphi_j, s_l) : \varphi_j = 2\pi j/P,\ s_l = d\,l,\ j = 0, \ldots, P-1,\ l \in \mathbb{Z}\}$$

which is obtained by letting $N = 0$, and the interlaced lattice

$$\mathbf{L}_I = \{(\varphi_j, s_{jl}) : \varphi_j = 2\pi j/P,\ s_{jl} = d(l\ + j/2),\ j = 0, \ldots, P-1,\ l \in \mathbb{Z}\}.$$

where P is even and $N = P/2$. We see that for the standard lattice the values $s_l = dl$ do not change with the angle φ_j. For the interlaced lattice the set of values $s_{jl} = dl + dj/2$ is shifted by $d/2$ when going from one angle φ_j to the next.

In practice one chooses $P = 2p$ for both lattices, and for the interlaced lattice one lets p be even. Then, because of the symmetry relation

$$Rf(\varphi, s) = Rf(\varphi + \pi, -s), \tag{3.4}$$

only the angles $\varphi_j \in [0, \pi)$ need to be measured. It turns out [12] that among all admissible lattices the standard and interlaced lattices are the only ones which fully exploit this symmetry.

The parameterization given in Lemma 1 is not unique. Alternative parameterizations of admissible sampling lattices have been used in [8] and [11].

We now wish to apply Shannon sampling theory in order to find the best sampling lattices. In order to do this we need some Fourier analysis for functions defined on the group $\mathbb{T} \times \mathbb{R}$. The Fourier transform on $\mathbb{T} \times \mathbb{R}$ is defined by

$$\hat{g}(k, \sigma) = (2\pi)^{-1} \int_0^{2\pi} \int_{\mathbb{R}} g(\varphi, s) e^{-i(k\varphi + \sigma s)}\, d\varphi\, ds, \quad k \in \mathbb{Z}, \sigma \in \mathbb{R}.$$

Using the notation $z = (\varphi, s)$, $\zeta = (k, \sigma)$, $\langle z, \zeta \rangle = k\varphi + \sigma s$, this can be written as

$$\hat{g}(\zeta) = (2\pi)^{-1} \int_{\mathbb{T}\times\mathbb{R}} g(z) e^{-i\langle z, \zeta\rangle} dz, \quad \zeta \in \mathbb{Z} \times \mathbb{R}.$$

The inverse Fourier transform in this setting is given by

$$\begin{aligned} \tilde{G}(\varphi, s) &= (2\pi)^{-1} \sum_{k\in\mathbb{Z}} \int_{\mathbb{R}} G(k, \sigma) e^{i(k\varphi + \sigma s)} d\sigma \\ &= (2\pi)^{-1} \int_{\mathbb{Z}\times\mathbb{R}} G(\zeta) e^{i\langle z, \zeta\rangle} d\zeta, \end{aligned}$$

with $z = (\varphi, s) \in \mathbb{T} \times \mathbb{R}$ and $\zeta = (k, \sigma) \in \mathbb{Z} \times \mathbb{R}$. Very useful tools for our purpose are the Poisson summation formulas for $\mathbb{R}$ and $\mathbb{T} \times \mathbb{R}$:

Theorem 3.1. *(Poisson summation formula for $\mathbb{R}$) Let $h > 0$ be fixed, and $g \in C(\mathbb{R})$ such that $|g(x)| \le C(1+|x|)^{-1-\epsilon}$, and $|\hat{g}(\sigma)| \le C(1+|\sigma|)^{-1-\epsilon}$ for some $C, \epsilon > 0$. Then*

$$(2\pi)^{-1/2} h \sum_{l\in\mathbb{Z}} g(x+hl) e^{-i\sigma(x+hl)} = \sum_{l\in\mathbb{Z}} \hat{g}(\sigma + 2\pi l/h) e^{ix2\pi l/h}. \tag{3.5}$$

For a proof see, e.g., [14, Theorem (8.36)].

The result holds also under less restrictive hypotheses: Let $g \in L_2(\mathbb{R})$ such that $\sum_{l\in\mathbb{Z}} |g(hl)|^2 < \infty$, and $\hat{g} \in L_1(\mathbb{R})$. Then (3.5) with $x = 0$ holds for almost every σ and the sums converge in $L_2([-\pi/h, \pi/h])$. This is a special case of a very general result given in [15, p. 217].

In order to state the Poisson summation formula for $\mathbb{T}\times\mathbb{R}$ we note that an admissible sampling lattice $\mathbf{L}$ has a corresponding "reciprocal lattice" $\mathbf{L}^\perp$ in the Fourier domain. $\mathbf{L}^\perp$ is the set of all $\eta \in \mathbb{Z}\times\mathbb{R}$ such that $\langle y, \eta\rangle \in 2\pi\mathbb{Z}$ for all $y \in \mathbf{L}$. From (3.3) it follows that

$$\mathbf{L}^\perp(d, N, P) \;=\; \{(Pk_1 - Nk_2,\; 2\pi k_2/d)\,,\;\; k_1, k_2 \in \mathbb{Z}\}. \tag{3.6}$$

Theorem 3.2. *(Poisson summation formula for $\mathbb{T}\times\mathbb{R}$) Let $z \in \mathbb{T}\times\mathbb{R}$ and $\zeta \in \mathbb{Z}\times\mathbb{R}$ be fixed, $\mathbf{L} = \mathbf{L}(d, N, P)$ be a an admissible lattice and $g \in C_0^\infty(\mathbb{T}\times\mathbb{R})$. Define the lattice constant $c_\mathbf{L}$ by $c_\mathbf{L} = d/P$. Then*

$$c_\mathbf{L} \sum_{y\in\mathbf{L}} g(z+y) e^{-i\langle z+y,\zeta\rangle} = \sum_{\eta\in\mathbf{L}^\perp} \hat{g}(\zeta+\eta) e^{i\langle z,\eta\rangle}. \tag{3.7}$$

We are now ready to state the classical sampling theorem for this setting; cf. [24].

Theorem 3.3. *Let $g \in C_0^\infty(\mathbb{T}\times\mathbb{R})$, $\mathbf{L} = \mathbf{L}(d, N, P)$ an admissible sampling lattice and K be a compact subset of $\mathbb{Z}\times\mathbb{R}$ such that its translates $K+\eta, \eta \in L^\perp$ are disjoint. Let χ_K denote the characteristic function of K, i.e., $\chi_K(\zeta) = 1$ if $\zeta \in K$ and $\chi_K(\zeta) = 0$ otherwise. For $z \in \mathbb{T}\times\mathbb{R}$ define*

$$Sg(z) = \frac{d}{P} \sum_{y\in L} \tilde{\chi}_K(z-y) g(y). \tag{3.8}$$

Then

$$|g(z) - Sg(z)| \;\;\le\;\; \pi^{-1} \int_{(\mathbb{Z}\times\mathbb{R})\setminus K} |\hat{g}(\zeta)| d\zeta. \tag{3.9}$$

Observe that if $\hat{g}$ vanishes outside of K then $g = Sg$, i.e., g can be recovered exactly from its samples on the lattice $\mathbf{L}$. The meaning of Sg and $\tilde{\chi}_K$ may become more clear by a comparison with the better known case of sampling on $\mathbb{R}$. A lattice is then an equidistant set $\mathbf{L} = d\mathbb{Z} = \{dl,\; l \in \mathbb{Z}\}$. Assume that K is an interval, say $K = [-1, 1]$. Then

$$\tilde{\chi}_K(x) \;=\; (2\pi)^{-1/2} \int_{-1}^{1} e^{ix\xi}\, d\xi \;=\; \sqrt{\frac{2}{\pi}}\, \frac{\sin x}{x} \;=\; \sqrt{\frac{2}{\pi}}\, \mathrm{sinc}(x),$$

with the "sinus cardinalis" $\operatorname{sinc}(x) = \sin(x)/x$. In this case Sg is the so-called cardinal series

$$Sg(x) = \frac{d}{\pi} \sum_{l \in \mathbb{Z}} g(dl) \operatorname{sinc}(x - dl).$$

The main idea of the proof of Theorem 3.3 is as follows: Using the Poisson summation formula (3.7) we may compute the Fourier transform of Sg as follows.

$$\begin{aligned} \widehat{Sg}(\zeta) &= \frac{d}{P} \sum_{y \in \mathbf{L}} g(y) \frac{1}{2\pi} \int_{\mathbb{T} \times \mathbb{R}} \tilde{\chi}_K(z - y) e^{-i\langle z, \zeta \rangle} dz \\ &= \chi_K(\zeta) \frac{d}{P} \sum_{y \in \mathbf{L}} g(y) e^{-i\langle y, \zeta \rangle} \\ &= \chi_K(\zeta) \sum_{\eta \in \mathbf{L}^\perp} \hat{g}(\zeta + \eta). \end{aligned} \tag{3.10}$$

From the Fourier inversion formula it follows that

$$|(g - Sg)(z)| \leq (2\pi)^{-1} \int_{\mathbb{Z} \times \mathbb{R}} |(\hat{g} - \widehat{Sg})(\zeta)| d\zeta.$$

Now we use (3.10) and observe that

$$(\hat{g} - \widehat{Sg})(\zeta) = \sum_{0 \neq \eta \in \mathbf{L}^\perp} \hat{g}(\zeta + \eta) \quad \text{for } \zeta \in K,$$

and $\widehat{Sg}(\zeta) = 0$ for $\zeta \notin K$. Hence

$$\begin{aligned} 2\pi |(g - Sg)(z)| &\leq \int_K |(\hat{g} - \widehat{Sg})(\zeta)| d\zeta \quad + \quad \int_{(\mathbb{Z} \times \mathbb{R}) \setminus K} |(\hat{g} - \widehat{Sg})(\zeta)| d\zeta \\ &\leq \sum_{0 \neq \eta \in \mathbf{L}^\perp} \int_K |\hat{g}(\zeta + \eta)| \; d\zeta \quad + \quad \int_{(\mathbb{Z} \times \mathbb{R}) \setminus K} |\hat{g}(\zeta)| d\zeta \\ &= \sum_{0 \neq \eta \in \mathbf{L}^\perp} \int_{K + \eta} |\hat{g}(\zeta)| d\zeta \quad + \quad \int_{(\mathbb{Z} \times \mathbb{R}) \setminus K} |\hat{g}(\zeta)| d\zeta \\ &\leq 2 \int_{(\mathbb{Z} \times \mathbb{R}) \setminus K} |\hat{g}(\zeta)| d\zeta \end{aligned} \tag{3.11}$$

where the last estimate follows from the disjointness of the sets $K + \eta$, $\eta \in \mathbf{L}^\perp$. For a complete proof see, e.g., [8] or [19, pp. 62–64].

We see from (3.10) that $\widehat{Sg}(\zeta)$ vanishes outside K. On the other hand the terms with $\eta \neq 0$ in the sum cause high frequencies in $\hat{g}$ to contribute to $\widehat{Sg}(\zeta)$ for $\zeta \in K$. This effect is called aliasing. The right-hand side of (3.9) provides an estimate for the so-called aliasing error. If g is the Radon transform of a function with compact support, then the Fourier transform $\hat{g}$ cannot have compact support

and an aliasing error will always be present. Thus tomography provides reasons to seek sharper estimates for the aliasing error than the classical estimate (3.9). In the remainder of this section we will report on a way to improve the estimate (3.9). These results were derived in [11] and are presented here for their relevance to sampling theory but will not be used further on, so that readers not interested in this topic may safely proceed to the next section.

Definition 3.1. For $g : \mathbb{T} \times \mathbb{R} \to \mathbb{C}$ and $\varphi \in \mathbb{T}$ let $g_\varphi : \mathbb{R} \to \mathbb{C}$ be given by $g_\varphi(s) = g(\varphi, s)$. Define

$$\epsilon^*(g, \tau) = (2\pi)^{-1/2} \sup_{\varphi \in \mathbb{T}} \int_{|\sigma|>\tau} |\widehat{g_\varphi}(\sigma)|\, d\sigma. \tag{3.12}$$

For $K \in \mathbb{Z} \times \mathbb{R}$ compact let $k_1 = \max\{|k| : (k, \sigma) \in K\}$, $\sigma_1 = \max\{|\sigma| : (k, \sigma) \in K\}$, and $M_1 = \{(k, \sigma) \in \mathbb{Z} \times \mathbb{R} : |\sigma| \le \sigma_1\} \backslash K$; see Figure 1.

Finally, for $a \in \mathbb{R}$ let $\lfloor a \rfloor$ and $\lceil a \rceil$ denote the largest integer $\le a$ and the smallest integer $\ge a$, respectively.

We first state a simplified version of the sharper estimate; cf. [11, Proposition 5]:

Proposition 3.1. *Let K be a compact subset of $\mathbb{Z} \times \mathbb{R}$ satisfying the condition that if $(k, \sigma) \in K$, then $(k', \sigma) \in K$ for all k' with $|k'| \le |k|$. Let $L = L(d, N, P)$ be an admissible sampling lattice such that the translated sets $K + \eta$, $\eta \in L^\perp$ are disjoint, $g \in C_0^\infty(\mathbb{T} \times \mathbb{R})$, Sg as in (3.8), $z \in \mathbb{T} \times \mathbb{R}$, and $k_1, \sigma_1, M_1, \epsilon^*$ as in Definition 3.1. Then*

$$|g(z) - Sg(z)| \quad \le \quad \pi^{-1} \int_{M_1} |\hat{g}(\zeta)| d\zeta \; + \; C(k_1, P)\, \epsilon^*(g, \sigma_1)$$

with $C(k_1, P) = 1 + \left(1 + \frac{6k_1+3}{P} + \frac{2}{\pi} \ln(4k_1 + 2)\right) \left\lceil \frac{\sigma_1 d}{\pi} \right\rceil$.

Proposition 3.1 is a corollary of Theorem 3.4 below. The key idea of the proof the Theorem is as follows. The Fourier inversion formula gives

$$\begin{aligned} |g(z) - Sg(z)| &= \frac{1}{2\pi} \left| \int_{\mathbb{Z}\times\mathbb{R}} (\hat{g}(\zeta) - \widehat{Sg}(\zeta))\, e^{i\langle z,\zeta\rangle}\, d\zeta \right| \\ &\le \frac{1}{2\pi} \left| \int_K (\hat{g}(\zeta) - \widehat{Sg}(\zeta))\, e^{i\langle z,\zeta\rangle}\, d\zeta \right| \\ &\quad + \frac{1}{2\pi} \left| \int_{(\mathbb{Z}\times\mathbb{R})\backslash K} \hat{g}(\zeta) e^{i\langle z,\zeta\rangle}\, d\zeta \right| \end{aligned} \tag{3.13}$$

where we have used that according to (3.10) $\widehat{Sg}$ vanishes outside K. The more

difficult term to estimate is the integral over K. By (3.10) we have

$$\begin{aligned} & \frac{1}{2\pi}\left|\int_K (\hat{g}(\zeta)-\widehat{Sg}(\zeta))e^{i\langle z,\zeta\rangle}\,d\zeta\right| \\ = \;& \frac{1}{2\pi}\left|\int_K \sum_{0\neq\eta\in\mathbf{L}^\perp} \hat{g}(\zeta+\eta)e^{i\langle z,\zeta\rangle}\,d\zeta\right| \end{aligned} \tag{3.14}$$

Now we use (3.6)to write

$$\sum_{0\neq\eta\in\mathbf{L}^\perp} \hat{g}(\zeta+\eta) \;=\; \sum_{(k_1,k_2)\neq(0,0)} \hat{g}(\zeta_1+Pk_1-Nk_2,\zeta_2+2\pi k_2/d).$$

The key idea is now to use the one-dimensional Poisson summation formula for the sum over k_1. This is possible for those $\zeta\in K$ and k_2 such that $|\zeta_2+2\pi k_2/d|>\sigma_1$, which guarantees that $\zeta+\eta\in M_2$ for all k_1. The detailed proof is given in [11].

We conclude by stating the more general result.

Theorem 3.4. *([11]) Let $g\in C_0^\infty(\mathbb{T}\times\mathbb{R})$, $K\subset\mathbb{Z}\times\mathbb{R}$ compact and $L=L(d,P,M,N)$ an admissible sampling lattice such that the translated sets $K+\eta$, $\eta\in L^\perp$ are disjoint. Let k_1,σ_1,M_1 as in Definition 3.1, $\sigma^*=\max\{\sigma_1,\ \frac{2\pi}{d}-\sigma_1\}$, and $\varphi_j=2\pi j/P$, $j=0,\dots P-1$. Then*

$$\begin{aligned} & |g(\varphi,s)-Sg(\varphi,s)| \\ \leq \;& \pi^{-1}\int_{M_1}|\hat{g}(\zeta)|d\zeta \;+\; (2\pi)^{-1/2}\int_{\sigma>\sigma_1}|\widehat{g_\varphi}(\sigma)|\,d\sigma \\ & + \frac{C(K,P,\varphi)}{\sqrt{2\pi}}\left\lceil\frac{\sigma_1 d}{\pi}\right\rceil \max_{j=0,\dots,P-1}\int_{|\sigma|>\sigma^*}|\widehat{g_{\varphi_j}}(\sigma)|d\sigma \end{aligned} \tag{3.15}$$

with

$$C(K,P,\varphi) \;=\; \frac{1}{P}\sum_{j=0}^{P-1}\max_{|\sigma|\leq\sigma_1}\left|\sum_{k\in N(\sigma)} e^{ik(\varphi-\varphi_j)}\right|.$$

where $N(\sigma)=\{k:\ (k,\sigma)\in K\}$.

4 The support of $\widehat{Rf}$

Theorem 3.3 indicates what needs to be done in order to find efficient sampling schemes for tomography, i.e., when $g=Rf$. First we need to find a suitable set K so that the right-hand side of (3.9) is sufficiently small. Then we need to identify lattices $L(d,N,P)$ as sparse as possible but such that the translated sets $K+\eta$, $\eta\in\mathbf{L}^\perp$ are disjoint.

The set K will of course depend on the function f. The crucial parameter turns out to be a cut-off frequency b such that $|\hat{f}(\xi)|$ is sufficiently small for $|\xi| > b$. The parameter b may be viewed as an "essential bandwidth" of f. A suitable set K was first found by Lindgren and Rattey [18, 26]. Natterer [19] gave the following rigorous estimate.

Theorem 4.1. *[19, p. 71] For $b > 0$ and $0 < \vartheta < 1$ let*

$$K(\vartheta, b) = \big\{(k, \sigma) \in \mathbb{Z} \times \mathbb{R} : \ |\sigma| < b, \ |k| < \vartheta^{-1} \max(|\sigma|, (1-\vartheta)b)\big\}; \tag{4.16}$$

see Figure 2. Let $f \in C_0^\infty(\Omega)$. Then

$$\int_{(\mathbb{Z}\times\mathbb{R})\setminus K} |\widehat{Rf}(\zeta)|\, d\zeta \ \le \ \frac{8}{\pi^2 \vartheta} \int_{|\xi|>b} |\hat{f}(\xi)| d\xi + \ \| f \|_{L_1} \, \eta(\vartheta, b), \tag{4.17}$$

where $\eta(\vartheta, b)$ decreases exponentially with b, satisfying an estimate

$$0 \le \eta(\vartheta, b) \le C(\vartheta) e^{-\lambda(\vartheta) b} \tag{4.18}$$

with constants $C(\vartheta), \lambda(\vartheta) > 0$.

The set $K(\vartheta, b)$ is depicted in Figure 2. What will turn out to be crucial for finding efficient sampling lattices is the bow-tie like shape of K. We will briefly sketch the derivation to illustrate how this shape arises. We have

$$\begin{aligned}
\widehat{Rf}(k,\sigma) &= (2\pi)^{-1} \int_0^{2\pi} \int_{\mathbb{R}} Rf(\varphi, s) e^{-i(k\varphi + \sigma s)} \, d\varphi \, ds \\
&= (2\pi)^{-1/2} \int_0^{2\pi} \widehat{R_\varphi f}(\sigma) \, e^{-ik\varphi} \, d\varphi \\
&= \int_0^{2\pi} \hat{f}(\sigma\theta) \, e^{-ik\varphi} \, d\varphi \qquad (4.19) \\
&= (2\pi)^{-1} \int_{\mathbb{R}^2} f(x) \int_0^{2\pi} e^{-i\langle x, \sigma\theta\rangle - ik\varphi} \, d\varphi \, dx \qquad (4.20)
\end{aligned}$$

In deriving (4.19) we used the projection-slice theorem (2.2). From (4.19) we see that $|\widehat{Rf}(k,\sigma)|$ will be small for $|\sigma| > b$ if b is the "essential bandwidth" of f, i.e., if $|\hat{f}(\xi)|$ is sufficiently small for $|\xi| > b$. This explains the upper and lower boundaries of the set K; cf. Figure 2. To explain the bow-tie shape we continue by writing $x = |x|(\cos\psi, \sin\psi)$. This gives

$$\begin{aligned}
\widehat{Rf}(k,\sigma) &= (2\pi)^{-1} \int_{\mathbb{R}^2} f(x) \int_0^{2\pi} e^{-i\sigma|x|\cos(\varphi-\psi) - ik\varphi} \, d\varphi \\
&= i^k \int_{\mathbb{R}^2} f(x) e^{-ik\psi} J_k(-\sigma|x|) \, dx \qquad (4.21)
\end{aligned}$$

where we have used the integral representation

$$J_k(t) = \frac{i^{-k}}{2\pi} \int_0^{2\pi} e^{it\cos\varphi - ik\varphi} \, d\varphi \tag{4.22}$$

for the Bessel functions of the first kind $J_k(t)$, which can be found in [19, p. 197].

Let $0 \le \vartheta < 1$. Combining an upper bound for the Bessel functions found in [1, 9.1.63] with a derivation given in [19, p. 198] one obtains the estimate

$$|J_k(\vartheta k)| \le e^{-(|k|/3)(1-\vartheta^2)^{3/2}}. \tag{4.23}$$

It shows that $|J_k(t)|$ decays exponentially as $|k|$ increases beyond $|t|$.

Since $f(x)$ is assumed to vanish for $|x| > 1$ we now see from (4.21) and (4.23) that $|\widehat{Rf}(k,\sigma)|$ will decay rapidly as soon as $|k| > |\sigma|$. This explains the bow-tie shape of the set K. We see that it comes from the compact support of the function f and the decay properties of the Bessel functions. For a complete derivation see [19, pp. 71-73]. One can also choose to eliminate the parameter ϑ by setting it equal to 1, as was done in [23, §4.3]. On the one hand this simplifies the presentation. On the other, it is apparent from the estimate (4.23) that the result may be somewhat optimistic for situations where both $|k|$ and $|\sigma|$ are small and $|k|$ only slightly exceeds $|\sigma|$.

5 Sampling conditions

The next step in applying Theorem 3.3 is to find conditions for the lattice parameters d, N, P such that the translated sets $K(\vartheta, b) + \eta$, $\eta \in \mathbf{L}^\perp(d, N, P)$ are disjoint. This is a requirement for the reciprocal lattice to be sparse which means that the sampling lattice itself must be sufficiently dense.

We begin with the standard lattice, i.e., $N = 0$. In order to exploit the symmetry (3.4) we assume P to be even. According to (3.6) the reciprocal lattice is given by

$$\mathbf{L}_S^\perp \;=\; \mathbf{L}^\perp(d, 0, P) \;=\; \{(Pk_1,\; 2\pi k_2/d)\,,\;\; k_1, k_2 \in \mathbb{Z}\}.$$

From this we readily conclude that for $K = K(\vartheta, b)$ the sets $K + \eta = K + (Pk_1,\; 2\pi k_2/d)$ will be disjoint if and only if

$$d < \pi/b, \qquad P > 2b/\vartheta; \tag{5.24}$$

see Figure 3.

The translated sets in Figure 3 do not appear to be packed as densely as possible. Another arrangement corresponding to a different lattice may result in a denser packing, giving a denser reciprocal lattice and therefore a sparser sampling lattice. However, it is apparent from letting $k_1 = 1, k_2 = 0$ in (3.6) that the point $\eta = (P, 0)$ always belongs to $\mathbf{L}^\perp(d, N, P)$. For K and $K + (P, 0)$ not to overlap we need $P > 2b/\vartheta$. Hence the standard lattice is optimal in the sense that it does require only a minimal number of directions. Other lattices can only be more efficient overall by allowing values of d greater than π/b. This turns out to be the case for the interlaced lattice. The reciprocal lattice is now given by

$$\mathbf{L}_I^\perp \;=\; \{((2k_1 - k_2)P/2,\; 2\pi k_2/d)\,,\;\; k_1, k_2 \in \mathbb{Z}\},$$

where for reasons of making use of the symmetry (3.4) we assume P to be a multiple of 4. Now the translated sets $K(\vartheta, b) + \eta$ will be disjoint if either conditions (5.24) are satisfied, or if

$$\frac{\pi}{b} < d \leq \frac{2\pi}{b}, \quad p > \max\left(\frac{2\pi}{\vartheta d}, \frac{(2-\vartheta)b}{\vartheta}\right), \ p \text{ even}, \ \ P = 2p. \tag{5.25}$$

Figure 4 shows the case of optimally sparse sampling with the interlaced lattice, i.e., $d = 2\pi/b$, $P = 2b(2-\vartheta)/\vartheta$. We see that the interlaced lattice allows for a maximal detector spacing of $d = 2\pi/b$ which is twice as large as the maximum allowed for standard lattice, with only a moderate increase in P, since ϑ can often be chosen very close to 1. Hence we obtain the same theoretical resolution (as determined by the bandwidth b) with only little more than half the amount of data required for the standard lattice.

Sampling conditions for a general admissible sampling lattice $\mathbf{L}(d, N, P)$ have been given in [11].

6 The filtered backprojection algorithm

Having identified efficient sampling schemes the question remains how best to reconstruct from efficiently sampled data. In this section which is based on the presentations given in [8] and [12], we describe the most popular tomographic reconstruction algorithm and present an error analysis which indicates how to achieve good reconstructions. The filtered backprojection algorithm is based on the following approximate inversion formula.

Theorem 6.1. *Let $e \in L_2(\mathbb{R}^2)$ be a radial function such that $|\xi|^{1/2}\hat{e}(\xi) \in L_2(\mathbb{R}^2)$, and ψ the even function of one variable given by $\hat{e}(\xi) = (2\pi)^{-1}\psi(|\xi|)$. Let the associated convolution kernel k be given by $\hat{k}(\sigma) = \frac{1}{2}(2\pi)^{-3/2}|\sigma|\psi(\sigma)$. Then*

$$e * f(x) = \int_0^{2\pi} \int_{\mathbb{R}} k(\langle x, \theta\rangle - s) Rf(\varphi, s)\, ds\, d\varphi. \tag{6.26}$$

Proof. The relation (6.26) can be verified by writing $e * f$ as $e * f(x) = \int \hat{e}(\xi)\hat{f}(\xi)e^{i\langle x,\xi\rangle}d\xi$, expressing the integral in polar coordinates, and using the relation (2.2); see, e.g., [10].

If e is an approximate δ-function then (6.26) gives an approximate reconstruction formula for f.

Discretizing the integrals in equation (6.26) by using the trapezoidal rule yields the filtered backprojection algorithm. We derive the algorithm assuming the data are values $Rf(\varphi_j, s_{jl})$ of the Radon transform of f, sampled on an admissible sampling lattice $\mathbf{L}(d, N, P)$ as described in (3.3).

Discretizing (6.26) with the trapezoidal rule gives

$$\begin{aligned} e * f(x) &\simeq \frac{2\pi}{P} \sum_{j=0}^{P-1} Q_j(\langle x, \theta_j \rangle), \\ Q_j(t) &= d \sum_l k(t - s_{jl}) Rf(\varphi_j, s_{jl}), \end{aligned}$$

with φ_j, s_{jl} as in (3.3), and $\theta_j = (\cos\varphi_j, \sin\varphi_j)$. The reconstruction is usually computed for values of x on a rectangular grid $x_{m_1 m_2} = (m_1/M_1, m_2/M_2)$. Since computing the discrete convolution $Q_j(\langle x, \theta_j \rangle)$ for each occurring value of $\langle x, \theta_j \rangle$ would take too long, one first computes $Q_j(iH)$, $|i| \leq 1/H$, and then obtains an approximation $I_H Q_j(\langle x, \theta_j \rangle)$ for $Q_j(\langle x, \theta_j \rangle)$ by linear interpolation with stepsize H. We assume that

$$H = d/(N'm), \text{ with } 0 < m, N' \in \mathbb{Z}, \text{ and } N'N/P \in \mathbb{Z}. \tag{6.27}$$

This gives $H = d/m$ for the standard lattice ($N' = 1$) and $H = d/(2m)$ for the interlaced lattice ($N' = 2$). Then the effect of interpolating the convolution is the same as replacing the kernel k with the piecewise linear function $I_H k$ which interpolates k at the points Hl, $l \in \mathbb{Z}$; see, e.g., [8, p.84]. Hence the algorithm computes the function

$$\begin{aligned} f_R(x) &= \frac{2\pi}{P} \sum_{j=0}^{P-1} I_H Q_j(\langle x, \theta_j \rangle) \\ &= \frac{2\pi d}{P} \sum_{j=0}^{P-1} \sum_{l \in \mathbb{Z}} I_H k\left(\langle x, \theta_j \rangle - s_{jl}\right) Rf\left(\varphi_j, s_{jl}\right) \end{aligned} \tag{6.28}$$

A popular choice for the convolution kernel k is the so-called Shepp-Logan kernel whose Fourier transform is given by

$$\hat{k}(\sigma) = \frac{1}{2}(2\pi)^{-3/2} |\sigma| \operatorname{sinc}(\sigma\pi/(2b)) \, \chi_{[-b,b]}(\sigma); \tag{6.29}$$

cf. [19, pp.110-111]. Here we used the notation χ_M to denote the characteristic function of a set M, i.e, $\chi_M(x) = 1$ for $x \in M$ and $\chi_M(x) = 0$ otherwise.

In [12] the following error estimate was given. It builds on pioneering work in [16] and extensions in [8]. For an alternative estimate yielding convergence rates depending on the smoothness of f see [27].

Theorem 6.2. *Let $f \in C_0^\infty(\Omega)$, $g = Rf$, f_R be as in (6.28) with e and k as in Theorem 6.1 and in addition such that $\hat{k} \in L_1(\mathbb{R})$ and $\sum_{l \in \mathbb{Z}} |k(Hl)|^2 < \infty$. Let $M \subset \mathbb{Z} \times \mathbb{R}$ be compact and let g be sampled on an admissible sampling lattice $\mathbf{L}$ with parameters d, N, P such that the translates $M + \eta$, $\eta \in \mathbf{L}^\perp$ are disjoint. Then, for $b > 0$,*

$$f_R(x) = G_H * e * f(x) \; + \; E_1(x) \; + \; E_2(x) \; + \; E_3(x) \; + \; E_4(x)$$

with

$$\begin{aligned}
\widehat{G}_H(\xi) &= (2\pi)^{-1}\mathrm{sinc}^2(H|\xi|/2)\chi_{[0,b]}(|\xi|),\\
|E_1(x)| &\le \sqrt{2\pi}\frac{d}{P}\sum_{y\in\mathbf{L}}|g(y)|\int_{\mathbb{Z}\times\mathbb{R}\setminus M}|F(\zeta,x)|d\zeta,\\
|E_2(x)| &\le 2\sqrt{2\pi}\left(\max_{|\sigma|\le b}\left|\mathrm{sinc}^2(H\sigma/2)\hat{k}(\sigma)\right|\right)\int_{(\mathbb{Z}\times\mathbb{R})\setminus M}|\hat{g}(\zeta)|\,d\zeta,\\
|E_3(x)| &\le (2\pi)^{\frac{3}{2}}\sup_{\theta}\int_{-b}^{b}\left(1-\mathrm{sinc}^2(H\sigma/2)\right)|\hat{k}(\sigma)|\sum_{l\in\mathbb{Z}}\left|\hat{f}\left(\left(\sigma+\frac{2\pi l}{d}\right)\theta\right)\right|d\sigma\\
|E_4(x)| &\le 2(2+d)\sqrt{2\pi}\parallel f\parallel_\infty\int_{|\sigma|>b}|\hat{k}(\sigma)|d\sigma,
\end{aligned}$$

where $\mathrm{sinc}(s)=\sin(s)/s$ *and for* $\zeta=(l,\sigma)\in\mathbb{Z}\times\mathbb{R}$,

$$F(\zeta,x)=J_l(\sigma|x|)\,\mathrm{sinc}^2(H\sigma/2)\,\hat{k}(\sigma)\,\chi_{[-b,b]}(\sigma) \tag{6.30}$$

with J_l *denoting the Bessel functions of the first kind.*

The parameter b is a cut-off frequency and should be chosen such that $|\hat{f}(\xi)|$ is sufficiently small for $|\xi|>b$. G_H has bandwidth b and so G_H*e*f is a low-pass filtered approximation to f with bandwidth b. Application of the theorem to the standard and interlaced lattices requires to specify an appropriate set M; to find sampling conditions for the lattice parameters d,N,P which ensure that the translated sets $M+\eta$, $\eta\in\mathbf{L}^\perp$ are disjoint; and to find estimates for $\int_{\mathbb{Z}\times\mathbb{R}\setminus M}|F(\zeta,x)|d\zeta$ and for $\int_{(\mathbb{Z}\times\mathbb{R})\setminus M}|\hat{g}(\zeta)|\,d\zeta$. We will first consider the standard lattice.

For the standard lattice we let M be the rectangle $M_1(\vartheta,b)=\{(k,\sigma):|\sigma|\le b,\quad |k|\le b/\vartheta\}$. Note that M_1 contains the set $K(\vartheta,b)$ of Theorem 4.1, so we know that $\widehat{Rf}(\zeta)$ will be small outside of M_1 if b is chosen as the essential bandwidth of f. The larger set M_1 can be chosen here since it turns out that the conditions for the translates $M_1+\eta$ to be disjoint are the same as for the sets $K+\eta$ to be disjoint. As we will see, having a larger set allows for a sharper error estimate. For the standard lattice we have $N=0$ in (3.3), and the reciprocal lattice $\mathbf{L}^\perp$ equals $\mathbf{L}^\perp=\{(Pk_1,\ 2\pi k_2/d),\ k_1,k_2\in\mathbb{Z}\}$. For reasons of efficiency as discussed earlier we let $P=2p$ be even. It is obvious that the translated sets $M_1(\vartheta,b)+\eta$, $\eta\in\mathbf{L}^\perp$ are disjoint if and only if the sampling conditions (5.24) are satisfied. Since $M_1(\vartheta,b)\supset K(\vartheta,b)$ the estimate of Theorem 4.1 can be used for $\int_{(\mathbb{Z}\times\mathbb{R})\setminus M_1}|\hat{g}(\zeta)|\,d\zeta$:

$$\begin{aligned}
\int_{(\mathbb{Z}\times\mathbb{R})\setminus M_1}|\hat{g}(\zeta)|\,d\zeta &\le \int_{(\mathbb{Z}\times\mathbb{R})\setminus K}|\hat{g}(\zeta)|\,d\zeta\\
&\le \frac{8}{\pi^2\vartheta}\int_{|\xi|>b}|\hat{f}(\xi)|d\xi+\ \parallel f\parallel_{L_1}\eta(\vartheta,b). \qquad (6.31)
\end{aligned}$$

Hence the error E_2 will be small if f is "essentially bandlimited" with bandwidth b in the sense that $\int_{|\xi|>b} |\hat{f}(\xi)| d\xi$ is sufficiently small.

It was shown in [12] that for the standard lattice

$$\int_{\mathbb{Z}\times\mathbb{R}\setminus M_1(\vartheta,b)} |F(\zeta,x)| d\zeta \quad \leq \quad 4b \, (\max_{|\sigma|\leq b} |\hat{k}(\sigma)|) \, \frac{e^{-\beta b/\vartheta}}{1-e^{-\beta}},$$
$$\beta = (1-\vartheta^2|x|^2)^{3/2}/3 \tag{6.32}$$

Hence the error E_1 will decay exponentially with increasing b.

The error E_3 is caused by the interpolation step and usually not a concern when using the standard lattice. This can be explained as follows: Consider the common parameter choice $d = H = \pi/b$. Since $\hat{f}(\xi)$ is assumed to be small for $|\xi| > b$, only the term with $l = 0$ in the sum will be significant, i.e., we have for $|\sigma| \leq b$

$$\sum_{l\in\mathbb{Z}} \left| \hat{f}((\sigma + 2\pi l/d)\theta) \right| \; = \; \sum_{l\in\mathbb{Z}} \left| \hat{f}((\sigma + 2bl)\theta) \right| \; \simeq |\hat{f}(\sigma\theta)|.$$

Usually the density function f is non-negative so that $|\hat{f}(\sigma\theta)|$ has a sharply peaked maximum at $\sigma = 0$ and is very small for $|\sigma|$ close to b. In such a case the error E_3 will be small since the factor $1 - \mathrm{sinc}^2(H\sigma/2)$ is small exactly where $|\hat{f}(\sigma\theta)|$ is large.

The last error E_4 can be kept small by chosing the convolution kernel k such that $\int_{|\sigma|>b} |\hat{k}(\sigma)| d\sigma$ is small. Often one can use bandlimited k so that E_4 vanishes entirely. This is for example the case for the Shepp-Logan kernel (6.29).

In summary, for the standard lattice we expect a good reconstruction as long as the sampling conditions (5.24) are met. The interpolation stepsize H may be as large as d. The picture in the upper left of Figure 5 demonstrates this conclusion. It shows a reconstruction of the so-called Shepp-Logan phantom with $p = 420$, $d = H = 1/128$, and $b = \pi/d$. The phantom models the crossection of a human head by a superposition of 11 ellipses whose parameters can be found in [28]. The phantom has values between 0 and 1 but the display is such that values greater 0.07 are rendered white and values less than -0.07 are rendered black. This choice is made because we are interested mainly in the small differences of the features inside the "head". Note that the reconstruction is very smooth inside the head but not outside. This comes from the fact that the strongest artifacts tend to appear along tangents to boundaries with large density jumps. In this case the only large density jumps are associated with the "skull", and no tangent to a boundary of the skull passes through the interior of the head. Since we are interested only in the interior, this reconstruction is quite satisfactory.

For the interlaced lattice we let $M = K(\vartheta, b)$ as in (4.16). For this lattice $P = 2p$ and $N = P/2 = p$. We always let p be even, so that because of the symmetry relation (3.4) only the angles $\varphi_j \in [0, \pi)$ need to be measured. The reciprocal lattice is $\mathbf{L}^\perp = \{(p(2k_1 - k_2), 2\pi k_2/d), \; k_1, k_2 \in \mathbb{Z}\}$. We have already seen that the sets $K(\vartheta, b) + \eta$, $\eta \in \mathbf{L}^\perp$ are disjoint if either (5.24) or (5.25) are satisfied. Comparison of (5.24) and (5.25) shows that the interlaced lattice allows

to double the detector spacing d with only a small increase of p. It is therefore potentially up to almost twice as efficient as the standard lattice. An estimate for $\int_{(\mathbb{Z}\times\mathbb{R})\setminus K} |\hat{g}(\zeta)|\, d\zeta$ which controls the error term E_2 has already been given in (6.31). It was shown in [12] that for the interlaced lattice

$$\int_{\mathbb{Z}\times\mathbb{R}\setminus K(\vartheta,b)} |F(\zeta,x)| d\zeta \quad \leq \quad (\max_{|\sigma|\leq b} |\hat{k}(\sigma)|)\; 4\vartheta e^{-\beta b'} \left(\frac{1+b'}{1-e^{-\beta}} \;+\; \frac{e^{-\beta}}{(1-e^{-\beta})^2} \right)$$
$$b' = (1-\vartheta)b/\vartheta, \quad \beta = (1-\vartheta^2|x|^2)^{3/2}/3. \qquad (6.33)$$

As in the case of the standard lattice, the error E_1 decreases exponentially with b, although at a slower rate. Also, for $\vartheta|x|$ close to 1 we expect this error to be significantly larger than for the standard lattice, due to the term involving $(1-e^{-\beta})^2$.

As before the error E_4 is kept small by chosing the convolution kernel k appropriately.

Of greater concern, however, is the error E_3, which unlike as in the case of the standard lattice is now critical. Consider the choice of parameters $d = 2\pi/b$, $H = \pi/b$. Now the sum over l in the estimate for E_3 in Theorem 6.2 may have 3 significant terms for $|\sigma| < b$:

$$\sum_{l\in\mathbb{Z}} \left| \hat{f}((\sigma + 2\pi l/d)\theta) \right| \;=\; \sum_{l\in\mathbb{Z}} |\hat{f}((\sigma+bl)\theta)| \;\simeq\; |\hat{f}((\sigma-b)\theta)| + |\hat{f}(\sigma\theta)| + |\hat{f}((\sigma+b)\theta)|.$$

As discussed earlier, the contribution of the term $|\hat{f}(\sigma\theta)|$ is strongly attenuated by the factor $(1 - \mathrm{sinc}^2(H\sigma/2))$. However, this is not the case for the other two terms. E.g., let σ be close to b. Then, assuming again that $\hat{f}$ is large near the origin, $|\hat{f}((\sigma - b)\theta)|$ will be large and is not attenuated by the factor $(1 - \mathrm{sinc}^2(H\sigma/2))$ which will be close to 1. Therefore we expect considerable reconstruction errors for this choice of parameters. That this is indeed the case is demonstrated in [16, 8] and in the upper right image of Figure 5. Compared to the upper left image we used the interlaced lattice with $d = 1/64$ and as before reconstructed with an interpolation stepsize $H = 1/128$. Strong high-frequency errors render the image useless.

A complementary explanation for this strong sensitivity with respect to H was given in [8]. The sums with respect to j and l in (6.28) can be viewed as discretizations of the integrals with respect to φ and s in (6.26), respectively. If the sampling conditions (5.24) are satisfied, then both the inner and outer integral are approximated accurately by the respective sum. But in case of (5.25) the stepsize d may be too large for an accurate approximation of the inner integral. In this case the accuracy of the reconstruction depends on the cancellation of these errors during the subsequent summation with respect to j. If the interpolation is not accurate, this cancellation is prevented.

Hence when using the interlaced lattice one should choose $H \ll \pi/b$, so that $(1-\mathrm{sinc}^2(H\sigma/2))$ is small for $|\sigma| < b$. Typical choices in practice are $H = \pi/(16b)$ or smaller. This choice has been made in the lower left image of Figure 5. The

high-frequency errors are indeed removed, but it turns out that we also removed a welcome smoothing effect of the interpolation with larger stepsize and are left with an unwelcome high-frequency pattern stemming from the discontinuity of the Fourier transform (6.29) of the convolution kernel k at the cut-off frequency. This error can be removed by chosing a different kernel k whose Fourier transform tapers of to zero at $\sigma = \pm b$. However, this entails a certain loss of resolution as was demonstrated in [8]. A better possibility is to first interpolate the data onto the standard lattice and then perform the reconstruction from the interpolated data. This was done in [7] using the interpolation from the sampling theorem with very good results. In the lower right of Figure 5 we interpolated the data onto the standard lattice using bilinear interpolation. The reconstruction is comparable to the one in the upper left, although now we used only half as many sampled data. However, we will see in the next section that part of the advantage of the interlaced lattice is lost due to increased sensitivity with respect to undersampling in the φ variable.

In summary, we expect good reconstructions for the interlaced lattice for d close to the optimal value $2\pi/b$ if the sampling conditions (5.25) are satisfied and if either H is sufficiently small or the data are interpolated onto the standard lattice prior to reconstruction.

7 Analysis of the effects of undersampling

In this section we use sampling theory to analyze some effects of undersampling. By undersampling we mean a violation of the sampling conditions (5.24) or (5.25). First we present a qualitative discussion of why the interlaced lattice is more sensitive to undersampling than the standard lattice. Then we perform a more detailed analysis and gain insight into the location and strength of undersampling artifacts when using the filtered backprojection algorithm.

Let us begin by noting an intriguing difference in the structure of the sampling conditions (5.24) and (5.25) for the standard lattice and the interlaced lattice, respectively. The conditions for d and P in (5.24) are independent of each other and indeed could be derived by applying one-dimensional sampling theory to each of the variables separately. On the other hand the conditions (5.25) come from genuinely two-dimensional sampling theory, which is reflected in the fact that the condition for P involves d. This has the intriguing consequence that in some cases the condition can be violated by decreasing d, in spite of the fact that this makes the sampling lattice more dense. So we would have undersampling in spite of having sampled more data. Figure 6 illustrates such a case. Compared to Figure 4 we decreased d without changing P. This has the effect of moving the translated sets $K + \eta$ further apart in the vertical direction. As the figure shows the translated sets are no longer disjoint. Numerical experiments in [8, p. 97] confirmed that this results in inferior tomographic reconstructions. This can also be seen from a comparison of the top and bottom pictures in the right half

of Figure 10, which are discussed further in the next section. On the other hand, sampling more data by leaving d fixed and increasing P does not violate (5.25). In this case the translated sets $K+\eta$ in Figure 4 move further apart from each other in the horizontal direction and remain disjoint.

It turns out that part of the advantage of the interlaced lattice is lost due to increased sensitivity with respect to undersampling in the φ variable. This can be qualitatively explained as follows (cf. [23, p. 89, Remark 3]): Figure 7 shows the translated sets $K+\eta$ in case of the standard lattice with $P = 2b/\vartheta$, $d = \pi/b$. For illustrative purposes we have marked the point $\zeta = (-0.85b/\vartheta, -0.99b) \in K$ and its translates $\zeta + \eta$ with a $*$. Assume we wish to compute an approximation for the Fourier transform $\hat{g}(\zeta)$ from the values of g on a sampling lattice $\mathbf{L}$ by means of taking the discrete Fourier transform with respect to $\mathbf{L}$. The result would be $\hat{g}(\zeta) \simeq (d/P)\sum_{y\in\mathbf{L}} g(y)e^{-i\langle y,\zeta\rangle}$, i.e., just the left-hand side of the Poisson summation formula (3.7) for $z = 0$. According to the Poisson summation formula this is equal to

$$\sum_{\eta\in\mathbf{L}^\perp} \hat{g}(\zeta+\eta) \;=\; \hat{g}(\zeta) \;+\; \sum_{0\neq\eta\in\mathbf{L}^\perp} \hat{g}(\zeta+\eta).$$

If the translated points $\zeta+\eta$ lie outside K for $\eta \neq 0$ we may assume that their contribution is small, so that we obtain a good approximation for $\hat{g}(\zeta)$. This will be the case if the sampling conditions (5.24) are satisfied, as can be seen from Figure 7. In Figure 8 we have decreased P to $P = 0.8(2b/\vartheta)$, so that the sets $K+\eta$ are no longer disjoint. We see that one of translated points $\zeta+\eta$, $\eta \neq 0$ now lies within K, causing an aliasing error. However, it turns out that in most applications of tomography this error will be small. This is due to the fact that in most cases $f(x) \geq 0$ for all x, so that the Fourier transform $\hat{f}(\xi)$ is maximal at the origin and decays quickly away from the origin. Because of the projection-slice theorem (2.2) the same is true for $\hat{g}(k,\sigma) = \widehat{Rf}(k,\sigma)$. Since the only one of the translated points $\zeta+\eta$, $\eta \neq 0$ which lies in K lies near the lower right corner of K, i.e., far away from the origin, the resulting error is likely to be small in most cases. This explains the observation that for the standard lattice P can often be chosen smaller than required by (5.24) without significant degradation in the reconstructed images. For example, in order to obtain the visible artifacts in the middle left picture of Figure 10, which is discussed further below, we had to reduce P very significantly.

This situation is different for the interlaced lattice as Figure 9 shows. Compared to Figure 4 we have decreased P to $4/5$ of its required value. We have again marked the point $\zeta = (-0.85b/\vartheta, -0.99b) \in K$ and its translates. Again one of the translated points lies inside K, but this time very close to the origin, where $|\widehat{Rf}(k,\sigma)|$ is large. This causes a large error for the approximate value of $\widehat{Rf}(\zeta)$, indeed the error can be expected to be much larger than the exact value. Hence we expect to incur large high-frequency errors which may significantly degrade the reconstructed images; cf. the middle right picture in Figure 10. This concludes our qualitative discussion.

In the remainder of this section we build on results in [19, p. 105] and [12] by giving a quantitative discussion of artifacts caused by undersampling in the φ variable for the standard and interlaced lattices when using the filtered backprojection algorithm.

For the following discussion it suffices to neglect the effect of the interpolation and to assume that the convolution kernel k from Theorem 6.1 is bandlimited with bandwidth b, i.e., $\hat{k}(\sigma) = 0$ for $|\sigma| > b$. This is possible since it was shown in [12] that the contributions from the interpolation and from the high-frequency part of k can be estimated separately. Hence we assume that we reconstruct the function

$$f_R(x) \;=\; \frac{2\pi d}{P} \sum_{j=0}^{P-1} \sum_{l\in\mathbb{Z}} k(\langle x, \theta_j\rangle - s_{jl}) Rf(\varphi_j, s_{jl}).$$

For $x \in \Omega$ define the auxiliary function $q_x \in L_2(\mathbb{T}\times\mathbb{R})$ such that $q_x(-\varphi,-s) = k(\langle x,\theta\rangle - s)$, i.e., $q_x(\varphi,s) = k(\langle x,\omega\rangle + s)$ with $\omega = (\cos\varphi, -\sin\varphi)$. As before we use the notation $\varphi_j = 2\pi j/P$ and $\theta_j = (\cos\varphi_j, \sin\varphi_j)$, write $g(\varphi,s)$ for $Rf(\varphi,s)$, and in cases were we consider operations acting on the s-variable alone we may write $g_\varphi(s)$, $q_{x,\varphi}(s)$ for $g(\varphi,s)$ and $q_x(\varphi,s)$, respectively. For the following discussion we will also assume that f is essentially bandlimited with bandwidth b in the sense that $|\widehat{g_\varphi}(\sigma)|$ is negligibly small for $|\sigma| > b$.

Using $s_{jl} = dl + dNj/P$, expressing $q_{x,\varphi}$ as the inverse Fourier transform of $\hat{q}_{x,\varphi}$ and using the one-dimensional Poisson summation formula (3.5) we obtain

$$\begin{aligned}
f_R(x) &= \frac{2\pi d}{P} \sum_{j=0}^{P-1} \sum_{l\in\mathbb{Z}} q_x(-\varphi_j, -s_{jl}) g(\varphi_j, s_{jl}) \\
&= \frac{\sqrt{2\pi} d}{P} \sum_{j=0}^{P-1} \int_R \hat{q}_{x,-\varphi_j}(\sigma) \sum_{l\in\mathbb{Z}} g_{\varphi_j}(dl + dNj/P) e^{-i\sigma(dl+dNj/P)}\, d\sigma \\
&= \frac{2\pi}{P} \sum_{j=0}^{P-1} \int_R \hat{q}_{x,-\varphi_j}(\sigma) \sum_{l\in\mathbb{Z}} \widehat{g_{\varphi_j}}(\sigma + 2\pi l/d) e^{iNl\varphi_j}\, d\sigma. \qquad (7.34)
\end{aligned}$$

On the other hand we have from Theorem 6.1

$$\begin{aligned}
e * f(x) &= \int_0^{2\pi} \int_{\mathbb{R}} k(\langle x,\theta\rangle - s)\, g(\varphi,s) ds\, d\varphi \\
&= \int_0^{2\pi} \int_{\mathbb{R}} \hat{q}_{x,-\varphi}(\sigma)\, \widehat{g_\varphi}(\sigma)\, d\sigma\, d\varphi.
\end{aligned}$$

Treating the term with $l = 0$ in (7.34) separately gives the following decom-

position of the reconstruction error.

$$\begin{aligned} E(x) &= f_R(x) - e * f(x) = E_1(x) + E_2(x), \\ E_1(x) &= \frac{2\pi}{P} \sum_{j=0}^{P-1} \int_{\mathbb{R}} \hat{q}_{x,-\varphi_j}(\sigma)\, \widehat{g_{\varphi_j}}(\sigma)\, d\sigma \\ &\quad - \int_0^{2\pi} \int_{\mathbb{R}} \hat{q}_{x,-\varphi}(\sigma)\, \widehat{g_\varphi}(\sigma)\, d\sigma\, d\varphi, \qquad (7.35) \\ E_2(x) &= \sum_{l \neq 0} \frac{2\pi}{P} \sum_{j=0}^{P-1} \int_R \hat{q}_{x,-\varphi_j}(\sigma) \widehat{g_{\varphi_j}}(\sigma + 2\pi l/d) e^{iNl\varphi_j}\, d\sigma. \qquad (7.36) \end{aligned}$$

Clearly E_1 can be viewed as the error stemming from discretizing the integral with respect to φ. In order to proceed further we need the Poisson summation formula for $\mathbb{T}$ which reads

$$\begin{aligned} \frac{2\pi}{P} \sum_{j=0}^{P-1} G(\varphi_j) e^{-im\varphi_j} &= \sqrt{2\pi} \sum_{l \in \mathbb{Z}} \widehat{G}(m + Pl), \qquad (7.37) \\ \widehat{G}(l) &= \frac{1}{\sqrt{2\pi}} \int_0^{2\pi} G(\varphi) e^{-il\varphi}\, d\varphi \end{aligned}$$

for sufficiently smooth functions G. Using (7.37) for the function

$$G_l(\varphi) = \int_{\mathbb{R}} \hat{q}_{x,-\varphi}(\sigma)\, \widehat{g_\varphi}(\sigma + 2\pi l/d)\, d\sigma$$

gives

$$\begin{aligned} E_1(x) &= \sqrt{2\pi} \sum_{k \in \mathbb{Z}} \widehat{G_0}(Pk) - \int_0^{2\pi} G_0(\varphi)\, d\varphi \\ &= \sqrt{2\pi} \sum_{k \neq 0} \widehat{G_0}(Pk) \qquad (7.38) \\ E_2(x) &= \sqrt{2\pi} \sum_{l \neq 0} \sum_{k \in \mathbb{Z}} \widehat{G_l}(Pk - Nl). \qquad (7.39) \end{aligned}$$

The next task is to compute the Fourier coefficients $\widehat{G_l}(m)$. We have

$$\begin{aligned} \hat{q}_{x,-\varphi}(\sigma) &= \hat{k}(\sigma)\, e^{i\sigma\langle x,\theta\rangle} \\ \widehat{g_\varphi}(\sigma + 2\pi l/d) &= \frac{1}{\sqrt{2\pi}} \int_{\mathbb{R}^2} f(y)\, e^{-i(\sigma + 2\pi l/d)\langle y,\theta\rangle}\, dy. \end{aligned}$$

The second equation is clear from the projection-slice theorem (2.2). This leads to

$$\begin{aligned} \widehat{G_l}(m) &= \frac{1}{\sqrt{2\pi}} \int_0^{2\pi} \int_{\mathbb{R}} \hat{q}_{x,-\varphi}(\sigma)\, \widehat{g_\varphi}(\sigma + 2\pi l/d)\, d\sigma\, e^{-im\varphi}\, d\varphi \qquad (7.40) \\ &= \frac{1}{2\pi} \int_{\mathbb{R}^2} f(y) \int_{\mathbb{R}} \hat{k}(\sigma) \int_0^{2\pi} e^{i\langle \sigma x - (\sigma + 2\pi l/d)y, \theta\rangle - im\varphi}\, d\varphi\, d\sigma\, dy. \end{aligned}$$

Writing $z = \sigma x - (\sigma + 2\pi l/d)y$ as $z = |z|(\cos\psi, \sin\psi)$ and using the representation (4.22) for the Bessel function we obtain

$$\begin{aligned} |\widehat{G_l}(m)| &= \left| \int_{\mathbb{R}^2} f(y) \int_{\mathbb{R}} \hat{k}(\sigma) J_m(|\sigma x - (\sigma + 2\pi l/d)y|) e^{-im\psi}\, d\sigma\, dy \right| \\ &\leq \int_{-b}^{b} |\hat{k}(\sigma)| \int_{\Omega} |f(y) J_m(|\sigma x - (\sigma + 2\pi l/d)y|)|\, dy\, d\sigma. \end{aligned} \tag{7.41}$$

We now combine (7.40) and (7.41) to find conditions for $|\widehat{G_l}(m)|$ to be small. First we observe from (7.40) that the integrand may not be negligible only for those values of σ for which both

$$|\sigma| \leq b \quad \text{and} \quad |\sigma + 2\pi l/d| \leq b. \tag{7.42}$$

Combining this with the estimate (4.23) we find that $\widehat{G_l}(m)$ will be negligibly small if

$$|\sigma x - (\sigma + 2\pi l/d)y| \;\leq\; \vartheta |m| \tag{7.43}$$

for all $x \in \Omega$, all $y \in \mathrm{supp}(f)$, and all values of σ satisfying (7.42).

We are now ready to discuss the errors for specific lattices and begin with the standard lattice. We assume that the sampling condition for d is satisfied, i.e., $d \leq \pi/b$. It follows that the conditions (7.42) are only satisfied if $l = 0$ and $|\sigma| \leq b$. Hence E_2 will be small. The leading terms in the expansion (7.38) for E_1 are $\widehat{G_0}(\pm P)$. According to (7.43) these terms will be small if

$$|\sigma(x - y)| \;\leq\; \vartheta P$$

for all $x \in \Omega$, all $y \in \mathrm{supp}(f)$, and all $|\sigma| \leq b$. Since the maximum value for $|x - y|$, $x, y \in \Omega$ equals 2, this condition leads back to the sampling condition $P \geq 2b/\vartheta$. If f is supported in a region $|y| \leq r < 1$, then we have $|x - y| \leq (1 + r)$ and (7.43) holds for $P \geq (1 + r)b/\vartheta$.

We also obtain some information about the location of artifacts in case (7.43) is violated. Assume that $f(y)$ is concentrated near a point y_0. Then $|\sigma(x - y)|$ is maximal for $|\sigma| = b$ and x as far away from y_0 as possible. So we expect the artifacts to be strongest and to appear first near the part of the boundary of Ω which is opposite y_0. However, we see from (7.40) that the contribution to $\widehat{G_0}(\pm P)$ from values $|\sigma|$ close to b will not be large, since $\widehat{g_\varphi}(\sigma)$ can be expected to be small for $|\sigma|$ near b if $f(x)$ is a non-negative function. These expectations are consistent with practical experience. With the standard lattice P can often be chosen significantly smaller than $2b/\vartheta$ without much degradation in the image. This is also demonstrated by the following numerical experiment. Figure 10 shows various reconstructions of the function

$$f(y) = \left(1 - 100|y - y_0|^2\right)_+^3, \quad y_0 = (0.4,\, 0.7)$$

where the + symbol indicates that $f(y) = 0$ whenever $(1 - 100|y - y_0|^2) < 0$. Hence f is supported in the region $|y - y_0| \leq 0.1$. For all reconstructions of Figure 10 we chose $b = 32\pi$ and the interpolation stepsize $H = \pi/(8b) = 1/256$. We have to choose very small H because our goal is to obtain accurate reconstructions in the sense of a small l_2-error. In case of $H = d$ the additional filtering caused by the function G_H from Theorem 6.2 causes additional error. This situation is different from Figure 5. There the goal was not so much to minimize the l_2-error but to obtain optically pleasing images, so the additional smoothing caused by G_H was welcome. The reconstructions are computed on a 256×256 grid. Since we want to study small artifacts the display is such that values below -0.01 are rendered black and values above 0.01 are rendered white. The upper left picture shows a reconstruction with the standard lattice with $d = \pi/b = 1/32$ and $p = 112$. Here we let $p = P/2$ and only used the p directions covering a 180 degree range. Clearly the sampling conditions (5.24) are satisfied. The relative l_2-error of this reconstruction is 4.8%. Slight reduction of p does not lead to a visible distortion in the image. The middle left picture in Figure 10 shows a reconstruction where p is significantly reduced to $p = 50$. As predicted, the resulting artifacts are strongest near the boundary of Ω opposite y_0. The relative error is now 7.4%. The artifacts are still not very strong. While the maximum of the function $f(y)$ equals 1, the maximum value of the artifact equals only 0.0107.

We now turn to the interlaced lattice. If $d \leq \pi/b$ we have the same situation as discussed above for the standard lattice. More interesting is the case $\pi/b \leq d \leq 2\pi/b$ as permitted by (5.25). In this case the conditions (7.42) are satisfied by the following values of l and σ.

$$\begin{aligned} l = 0, &\qquad -b \leq \sigma \leq b \\ l = 1, &\qquad -b \leq \sigma \leq b - \frac{2\pi}{d} \\ l = -1, &\qquad \frac{2\pi}{d} - b \leq \sigma \leq b \end{aligned}$$

The terms with $l = 0$ lead to the same discussion as above, since the parameter d does not occur in (7.38). In the following we investigate the terms with $l = 1$. The terms with $l = -1$ lead to the same conclusions. For $l = 1$ the leading terms in the expansion (7.39) for E_2 are $\widehat{G_1}(\pm P/2)$. Recall that $N = P/2$ for the interlaced lattice. For these terms to be small we need

$$|\sigma x - (\sigma + 2\pi/d)y| \;\leq\; \vartheta P/2$$

all $x \in \Omega$, all $y \in \mathrm{supp}(f)$, and $-b \leq \sigma \leq b - 2\pi/d$. For these values of σ we obtain

$$\begin{aligned} |\sigma x - (\sigma + 2\pi/d)y| &\leq |\sigma|\,|x| \;+\; \left|\sigma + \frac{2\pi}{d}\right|\,|y| \\ &= |\sigma|\,|x| \;+\; \left(\frac{2\pi}{d} - |\sigma|\right)\,|y| \;\leq\; \frac{2\pi}{d}. \end{aligned} \tag{7.44}$$

where we have used that $b \leq 2\pi/d \leq 2b$ because of (5.25). This leads to the condition $P \geq 4\pi/(\vartheta d)$ for P which is consistent with the sampling condition (5.25). The upper right picture in Figure 10 shows a reconstruction using the interlaced lattice with $p = 112$ and $d = 2\pi/b = 1/16$. The sampling conditions (5.25) are satisfied and with a relative l_2-error of 4.7% the reconstruction is of equal accuracy as the one from the standard lattice in the upper left picture, although now we have only half as many sampled data.

Again we obtain some information about the magnitude and location of artifacts caused by choosing P too small. Assume again that $f(y)$ is concentrated near a point y_0. Then we have that $M(\sigma) = \max_{x\in\Omega} |\sigma x - (\sigma + 2\pi/d)y_0|$ will be maximal as σ runs through $[-b, b - 2\pi/d]$ if $\sigma = -b$. If d is chosen very close to $2\pi/b$, then for σ near $-b$ we have

$$|\sigma x - (\sigma + 2\pi/d)y| \simeq b|x|$$

since the term $(\sigma + 2\pi/d)y \simeq (\sigma + b)y$ will be negligible for σ close to $-b$. Hence for P too small we expect an artifact to appear in the ring-like region $\vartheta P/(2b) < |x| \leq 1$. This is indeed observed in the middle right picture of Figure 10, where we reduced $p = P/2$ slightly to $p = 100$.

The geometry of the artifacts is different when d is not very close to $2\pi/b$, so that the term $(\sigma + 2\pi/d)y$ is not negligible for σ close to $-b$. In this case $|\sigma x - (\sigma + 2\pi/d)y_0|$ will be maximal for $\sigma = -b$ and $x = y_0/|y_0|$. Hence we expect the strongest artifacts at the part of the boundary of Ω which is nearest y_0. This is shown in the bottom right picture of Figure 10 where we used $p = 112$ and decreased d to $d = 1/18$ so that the sampling condition $p > 2\pi/(\vartheta d)$ is violated. Clearly, the strongest artifacts are at the boundary of Ω near the support of f.

We also see from (7.40) that the contribution from values of σ near $-b$ to $\widehat{G_1}(\pm P/2)$ is not necessarily small. For example, if $d = 2\pi/b$ and $\sigma = -b$, then $\widehat{g_\varphi}(\sigma + 2\pi/d) = \widehat{g_\varphi}(0)$ which is usually large. Hence the errors from choosing P too small can be expected to be much larger as in case of the standard lattice. This is indeed observed in practice, as can be seen by comparing the relative errors in Figure 10.

8 Further developments

In this article we have only considered two dimensions and the so-called parallel-beam geometry. The results reported in the first six sections are a summary of research which has developed over a period of time, beginning with Cormack [3] and Lindgren and Rattey [26], and being further developed by Natterer [19, 20, 21, 22, 23], Kruse [16], Desbat [4] and the author [7, 8, 10, 11, 12].

Of great practical importance is also the so-called fan-beam geometry. Efficient sampling schemes for the fan-beam geometry have been derived by Natterer [20]; see also [19, 23].

Of growing interest are questions of sampling in three-dimensional tomography. For work in this area see, e.g., [5, 6, 22, 25].

Finally, in this article we only discussed applications of the classical sampling theorem. Some tomographic applications call for non-equidistant sampling and have stimulated research in this area, e.g., [2, 7, 9, 29].

References

[1] M. Abramowitz and I. A. Stegun *Handbook of Mathematical Functions,* U.S. Dept. of Commerce, 1972.

[2] H. Behmard and A. Faridani Sampling of bandlimited functions on unions of shifted lattices *J. Fourier Anal. Appl.* 8:43–58, 2002.

[3] A. M. Cormack Sampling the Radon transform with beams of finite width *Phys. Med. Biol.* 23:1141–1148, 1978.

[4] L. Desbat Efficient sampling on coarse grids in tomography, *Inverse Problems*, 9:251–269, 1993.

[5] L. Desbat Echantillonnage paralléle efficace en tomographie 3D. *C.R. Acad. Sci. Paris*, Sërie I, 324:1193-1199, 1997.

[6] L. Desbat Interpolation of lacking data in tomography, *Proceedings of SampTA 2001, Intern. Conference on Sampling Theory and Applications, May, 2001, Orlando, FL*, pp. 123-128, 2001.

[7] A. Faridani An application of a multidimensional sampling theorem to computed tomography *Contemporary Mathematics*, 113:65–80, 1990.

[8] A. Faridani Reconstructing from efficiently sampled data in parallel-beam computed tomography. *Inverse Problems and Imaging*, G.F. Roach (ed.), Pitman Research Notes in Mathematics Series, Vol. 245, Longman, 1991, pp. 68–102.

[9] A. Faridani A generalized sampling theorem for locally compact abelian groups *Math. Comp.* 63:307–327, 1994.

[10] A. Faridani Results, old and new, in computed tomography. *Inverse Problems in Wave Propagation*, G. Chavent et al. (editors), The IMA Volumes in Mathematics and its Applications, Vol. 90, Springer Verlag, New York, 1997, pp. 167-193.

[11] A. Faridani Sampling in parallel-beam tomography. *Inverse Problems, Tomography, and Image Processing*, A. G. Ramm (editor), Plenum, New York, 1998, pp. 33–53.

[12] A. Faridani and E. L. Ritman High-resolution computed tomography from efficient sampling. *Inverse Problems*, 16:635–650, 2000.

[13] A. Faridani, K. A. Buglione, P. Huabsomboon, O. D. Iancu, and J. McGrath Introduction to local tomography *Contemporary Mathematics* 278:29–47, 2001.

[14] G. B. Folland *Real Analysis*, Wiley, New York, 1984.

[15] K. Gröchenig Aspects of Gabor analysis on locally compact abelian groups. *Gabor Analysis and Algorithms*, H. G. Feichtinger and T. Strohmer (editors), Birkhäuser, Boston, 1998, pp. 211-231.

[16] H. Kruse Resolution of reconstruction methods in computerized tomography, *SIAM J. Sci. Stat. Comput.* 10:447–474, 1989.

[17] R. M. Lewitt, R. H. T. Bates, and T .M. Peters Image reconstruction from projections: II: Modified back-projection methods *Optik*, 50:85–109, 1978.

[18] A. G. Lindgren and P. A. Rattey The inverse discrete Radon transform with applications to tomographic imaging using projection data *Advances in Electronics and Electron Physics* 56:359–410, 1981.

[19] F. Natterer *The Mathematics of Computerized Tomography*, Wiley, 1986.

[20] F. Natterer Sampling in fan-beam tomography *SIAM J. Appl. Math.* 53:358–380, 1993.

[21] F. Natterer Recent developments in x-ray tomography *Tomography, Impedance Imaging, and Integral Geometry*, E.T. Quinto, M. Cheney, and P. Kuchment (eds.), Lectures in Applied Mathematics, Vol. 30, Amer. Math. Soc., 1994, pp. 177–198.

[22] F. Natterer Resolution and reconstruction for a helical CT scanner *Technical Report 20/96-N*, Mathematics Dept., University of Münster, Germany.

[23] F. Natterer and F. Wuebbeling, Mathematical Methods in Image Reconstruction, SIAM, Philadelphia, 2001.

[24] D. P. Petersen and D. Middleton Sampling and reconstruction of wave-number-limited functions in N-dimensional euclidean space. *Inf. Control* 5:279–323, 1962.

[25] V. P. Palamodov Localization of harmonic decomposition of the Radon transform *Inverse Problems* 11:1025–1030, 1995.

[26] P. A. Rattey and A. G. Lindgren Sampling the 2-D Radon transform. *IEEE Trans. Acoust. Speech Signal Processing* 29:994–1002, 1981.

[27] A. Rieder and A. Faridani The semi-discrete filtered backprojection algorithm is optimal *Preprint Nr. 02/06*, Institut für Wissenschaftliches Rechnen und Mathematische Modellbildung, Universität Karlsruhe, D-76128 Karlsruhe, Germany.

[28] S. W. Rowland Computer implementation of image reconstruction formulas *Image Reconstruction from Projections: Implementation and Applications*, G. T. Herman (ed.), Springer, 1979.

[29] D. Walnut Nonperiodic Sampling of Bandlimited Functions on Unions of Rectangular Lattices *J. Fourier Anal. Appl.* 2:435–452, 1996

Acknowledgment. This research was supported by NSF grant DMS-9803352.

Adel Faridani
Department of Mathematics
Oregon State University
Corvallis, Oregon 97331
USA
faridani@math.orst.edu

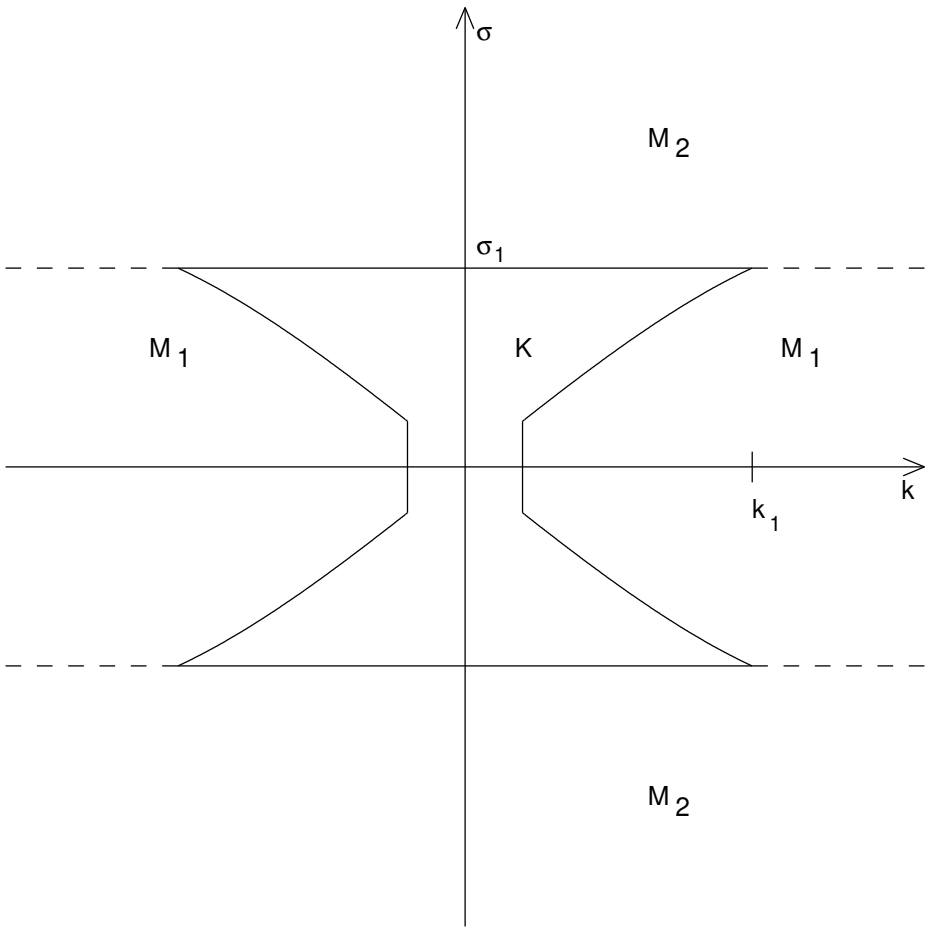

FIGURE 1. Example of a set K with the related quantities k_1, σ_1, M_1 as in Definition 3.1 and the set $M_2 = (\mathbb{Z} \times \mathbb{R}) \backslash (K \cup M_1)$.

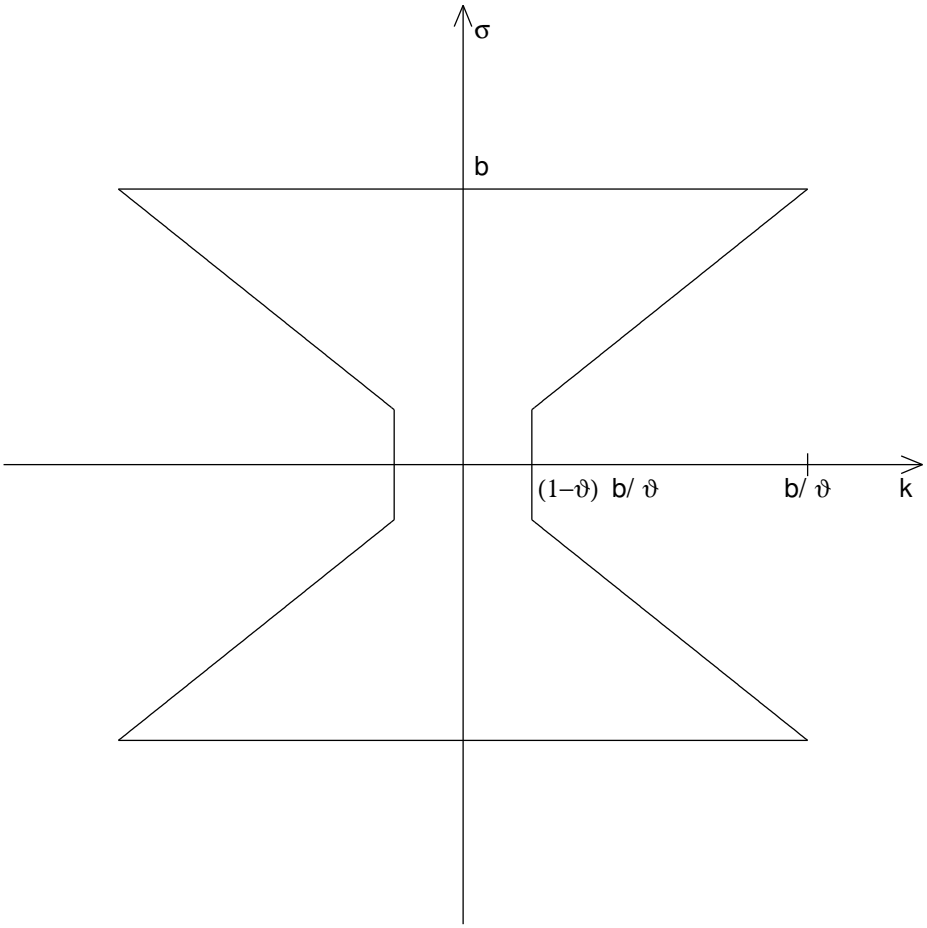

FIGURE 2. The set $K(\vartheta, b)$ for $\vartheta = 0.8$.

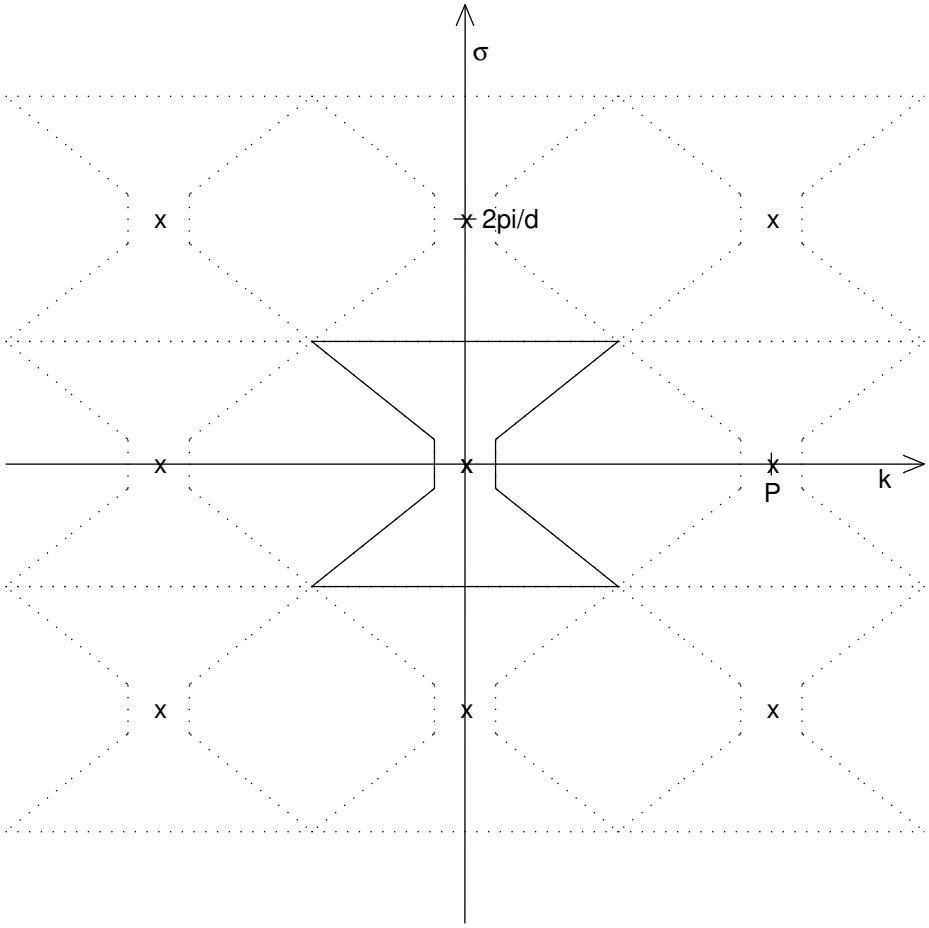

FIGURE 3. The translated sets $K + \eta$ for the standard lattice in case of $d = \pi/b$, $P = 2b/\vartheta$. The points η of the reciprocal lattice are indicated by an 'x'.

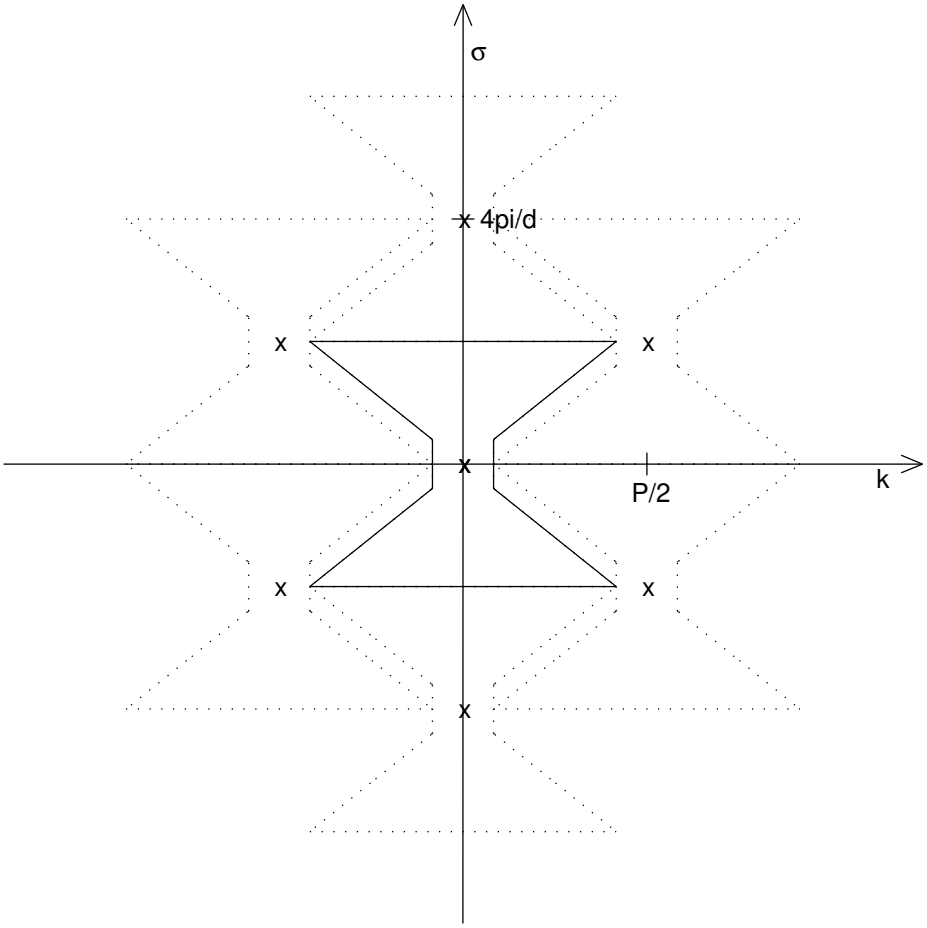

FIGURE 4. The translated sets $K + \eta$ for the interlaced lattice in case of $d = 2\pi/b$, $P = 2b(2 - \vartheta)/\vartheta$. The points η of the reciprocal lattice are indicated by an 'x'.

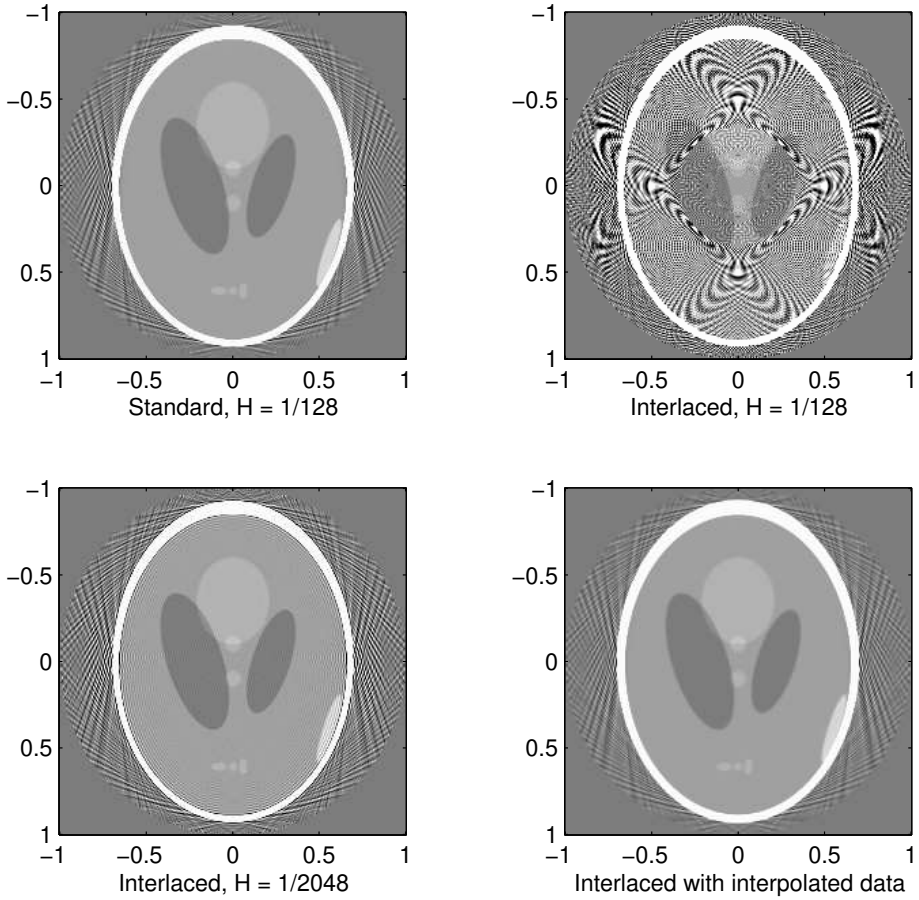

FIGURE 5. Reconstructions of the Shepp-Logan phantom. All reconstructions were computed with $p = 420$, $b = 128\pi$, and the Shepp-Logan convolution kernel (6.29). Upper left: Standard lattice, $d = H = 1/128$. Upper right: Interlaced lattice, $d = 1/64$, $H = 1/128$. Lower left: Interlaced lattice, $d = 1/64$, $H = 1/2048$. Lower right: Data sampled on interlaced lattice with $d = 1/64$ and then interpolated onto standard lattice with $d = 1/128$ using bilinear interpolation. Reconstruction from the interpolated data with $H = 1/128$.

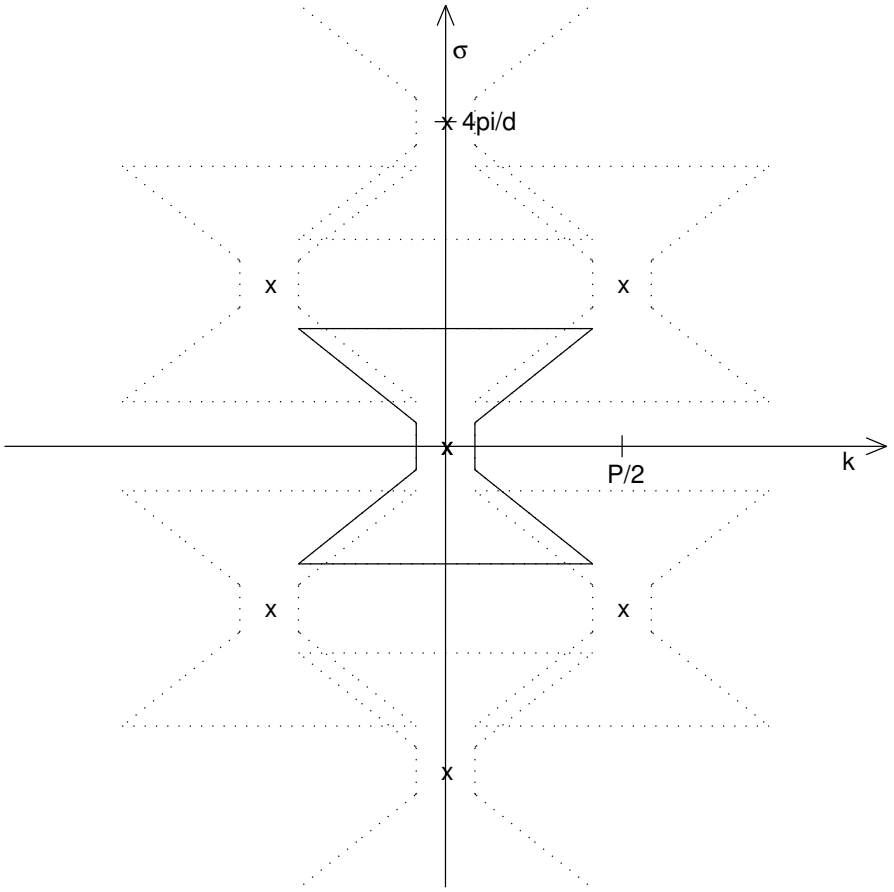

FIGURE 6. The translated sets $K + \eta$ for the interlaced lattice in case of $d = 1.45\pi/b$, $P = 2b(2 - \vartheta)/\vartheta$, $\vartheta = 0.8$. In spite of denser sampling than in the case $d = 2\pi/b$ depicted in Figure 4, the sets $K + \eta$ are no longer disjoint, resulting in aliasing error.

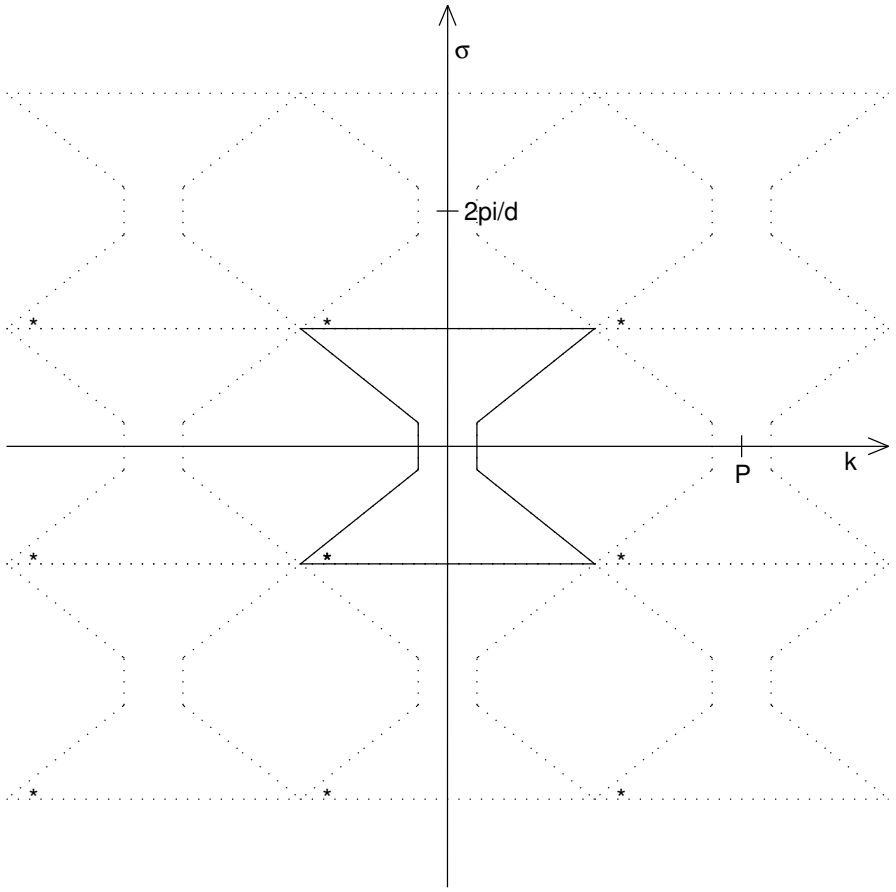

FIGURE 7. The translated sets $K + \eta$ for the standard lattice in case of $d = \pi/b$, $P = 2b/\vartheta$, $\vartheta = 0.8$. The point $\zeta = (-0.85b/\vartheta, -0.99b) \in K$ and its translates $\zeta + \eta$, $\eta \in \mathbf{L}^\perp$ are marked with a $*$.

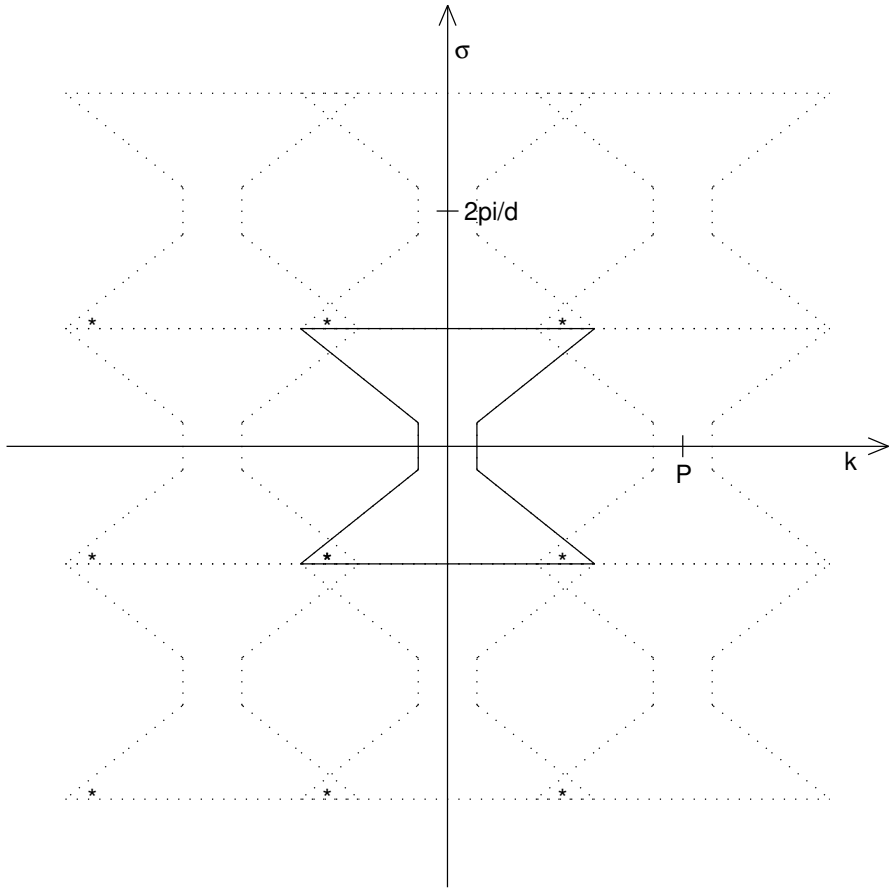

FIGURE 8. The translated sets $K + \eta$ for the standard lattice in case of $d = \pi/b$, $P = 0.8(2b/\vartheta)$, $\vartheta = 0.8$. The point $\zeta = (-0.85b/\vartheta, -0.99b) \in K$ and its translates $\zeta + \eta$, $\eta \in \mathbf{L}^{\perp}$ are marked with a $*$.

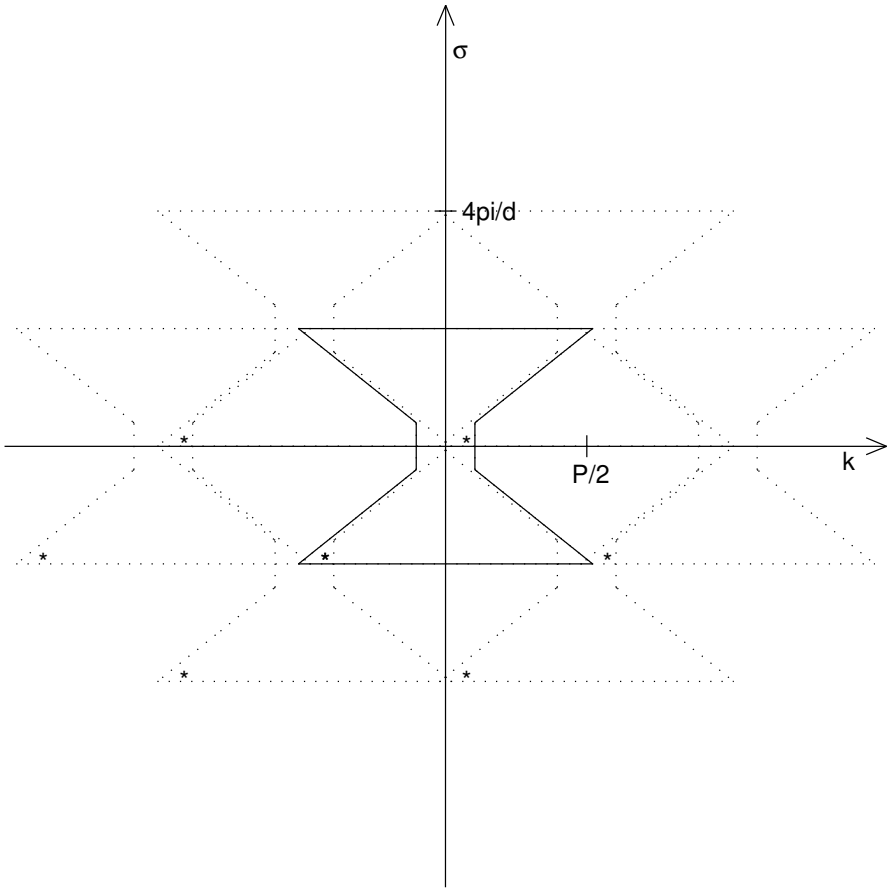

FIGURE 9. The translated sets $K + \eta$ for the interlaced lattice in case of $d = \pi/b$, $P = 0.8(2b(2-\vartheta)/\vartheta)$, $\vartheta = 0.8$. The point $\zeta = (-0.85b/\vartheta, -0.99b) \in K$ and its translates $\zeta + \eta$, $\eta \in \mathbf{L}^\perp$ are marked with a $*$.

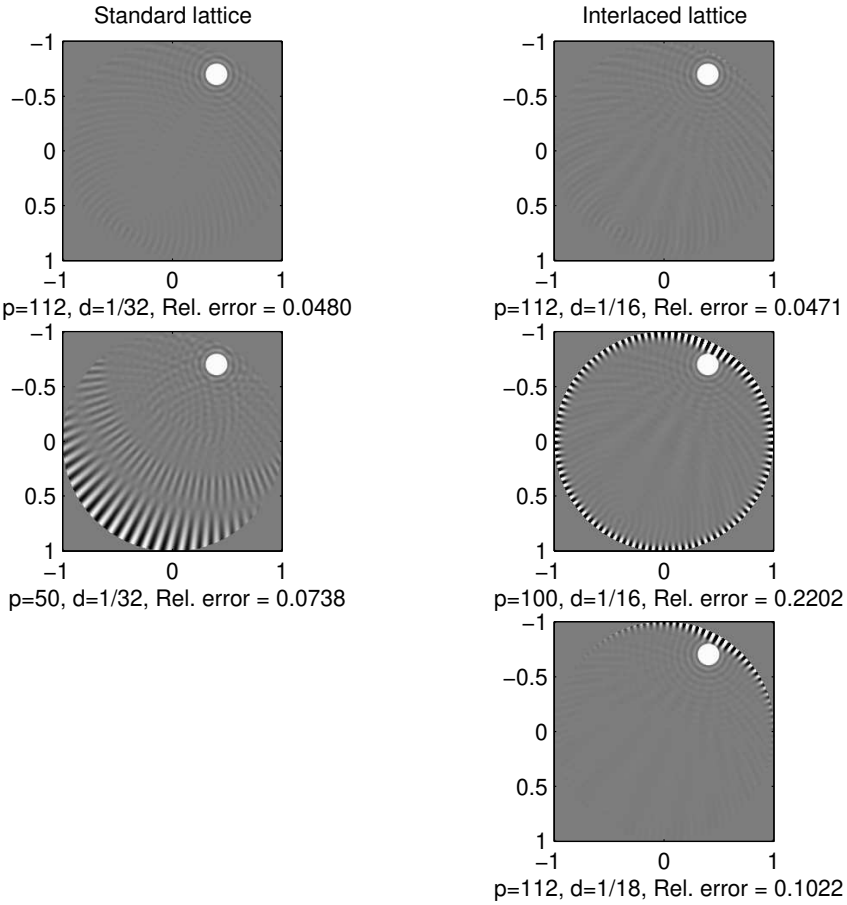

FIGURE 10. Artifacts resulting from P being too small. The function to be reconstructed is $f(y) = \left(1 - 100|y - y_0|^2\right)_+^3$, $y_0 = (0.4, 0.7)$. Reconstructions from the standard lattice are in the left column and from the interlaced lattice in the right column. All reconstructions are computed with $b = 32\pi$ and an interpolation stepsize $H = 1/256$ and displayed on a 256×256 grid such that values less than -0.01 are rendered black and values greater than 0.01 are rendered white.